Yaw and lateral predictive control in long combinations of heavy vehicles

Master of Science Thesis

MANSOUR KESHAVARZ BAHAGHIGHAT

Department of Signals and Systems
Division of Automatic Control, Automation and Mechatronics
CHALMERS UNIVERSITY OF TECHNOLOGY
Göteborg, Sweden, 2011
Report No. EX011/2010

Yaw and Lateral Predictive Control in Long Combinations of Heavy Vehicles

Master of Science Thesis

Author:

Mansour Keshavarz Bahaghighat

Supervisor:

Dr. Paolo Falcone

Department of Signals and Systems

Division of Automatic Control, Automation and Mechatronics

CHALMERS UNIVERSITY OF TECHNOLOGY

November 2010

Abstract

In this thesis work we have considered the problem of controlling the yaw and lateral dynamics in long combinations of heavy vehicles. Yaw and lateral instability in heavy vehicles is one of the main reasons of the traffic accidents involving this type of vehicles and it is even more critical in long combinations, i.e., a truck with multiple towed units. Such vehicle configurations, in lane change maneuvers, exhibit yaw rate and lateral acceleration amplifications, causing tail swings of the towed units.

The contribution of this thesis work is the design and the experimental validation of Predictive Control strategies aiming at reducing, via active steering, the Rearward Amplification (RWA) of the yaw dynamics in the two rearmost units in a truck-dolly-semitrailer combination.

We have experimentally validated the proposed approaches on a 60 tons, 25 meter long truck-dolly-semitrailer combination, with steering axles on the dolly and the semitrailer units. Experiments have been performed, consisting of single lane changes on a dry road up to 80 Km/h. The obtained results demonstrate the capability of the proposed approach of coordinating the steering at five axles in order to limit the yaw rate amplification, with reduced tuning efforts compared to algorithms based on classical approaches (e.g., PI controllers).

Acknowledgments

First of all, I would like to thank my supervisor, Paolo Falcone for providing me the opportunity to work on this interesting thesis work. His support and assistance guided me throughout this project.

Special thanks to my parents for all the support they provided me through my entire life, and in particular, during my studies abroad. Without their support and encouragement I would not have been worked conveniently.

I am very grateful to Dr. Leo Laine and M.Sc. Kristoffer Tagesson from Volvo 3P for valuable collaborations and creating friendly working environment.

I would like also to thank Dr. Mathias Lidberg, Goran Stigler and PhD. Sogol Kharrazi from the Department of Applied Mechanics and Dr. Brad Schofield from Modelon AB for their assistance and helpful discussions during this project.

Many thanks to Andrew Odhams and Richard Roebuck for their useful suggestions and feedbacks, especially during experimental testing.

I am thankful to my friend, Bruno Augusto, for all the granted aids and helpful hints during the real time implementations. Without his help, my task would surely be more complex.

Finally, I would like to thank all the people and friends who were not mentioned in this acknowledgment but helped me, directly or indirectly, during this work.

Contents

List of Figures

List of Tables

Nomenclature

m_1	Mass of truck
m_2	Mass of dolly
m_3	Mass of semitrailer
I_{z_1}	Moment of inertia of truck about vertical axis
I_{z_2}	Moment of inertia of dolly about vertical axis
I_{z_3}	Moment of inertia of semitrailer about vertical axis
l_{11}	Distance from front axle of truck to truck CG
l_{12}	Distance from truck CG to first rear axle
l_{13}	Distance from truck CG to tag axle
d_{1r}	Distance from truck CG to first articulation point
d_{2f}	Distance from frist articulation point to dolly CG
l_{21}	Distance from dolly CG to front axle of dolly
l_{22}	Distance from dolly CG to rear axle of dolly
d_{2r}	Distance from dolly CG to second articulation point
d_{3f}	Distance from frist articulation point to semitrailer CG
l_{31}	Distance from semitrailer CG to front axle of semitrailer
l_{32}	Distance from semitrailer CG to middle axle of semitrailer
l_{33}	Distance from semitrailer CG to rear axle of semitrailer
C_{ij}	Cornering stiffness of the *j-th* axle of the *i-th* unit
F_{xai}	Longitudinal force at *i-th* articulation joint

F_{yai}	Lateral force at *i-th* articulation joint
M_z	Moment about z axis
v_x	Longitudinal velocity for each of three units
v_{yi}	Lteral velocity of the *i-th* unit
α	Tire slip angle
β_i	Side slip angle of the *i-th* unit
δ_{11}	Steer angle of the truck
δ_2	Steer angle sor the dolly axles
δ_3	Steer angle for the semitrailer axles
θ_i	*i-th* Articulation angle

Chapter 1

Introduction

Heavy vehicles play an important role in supporting transportation sector. A big share of goods transportation is with trucks (alternative could be trains). On the other hand, reducing the number of the heavy trucks in the roads has been identified as a solution to reduce the emission caused by transport sector. So, in order to reduce the shipping cost and pollute less, it is convenient to use longer trucks in the roads [1],[13].

1.1 Long combination vehicles

Typically a LCV (Longer Combination Vehicle) consists of a truck with two or more trailers. Different combinations for heavy vehicles are illustrated in Figure 2.1. We note that all the combinations shown in Figure 2.1 exist in the reality.

In Europe, maximum overall length for a heavy vehicle combination is 18.75 meters with a maximum weight of 44 tons. Since 1997, Sweden and Finland have received exemption from this rule, which allows trucks in these countries to be up to 25.25 meters long based on the so-called modular concept with a maximum weight of 60 tons [2]. Nowadays in Norway, the Netherlands and Denmark these trucks have permission to commute on the roads.

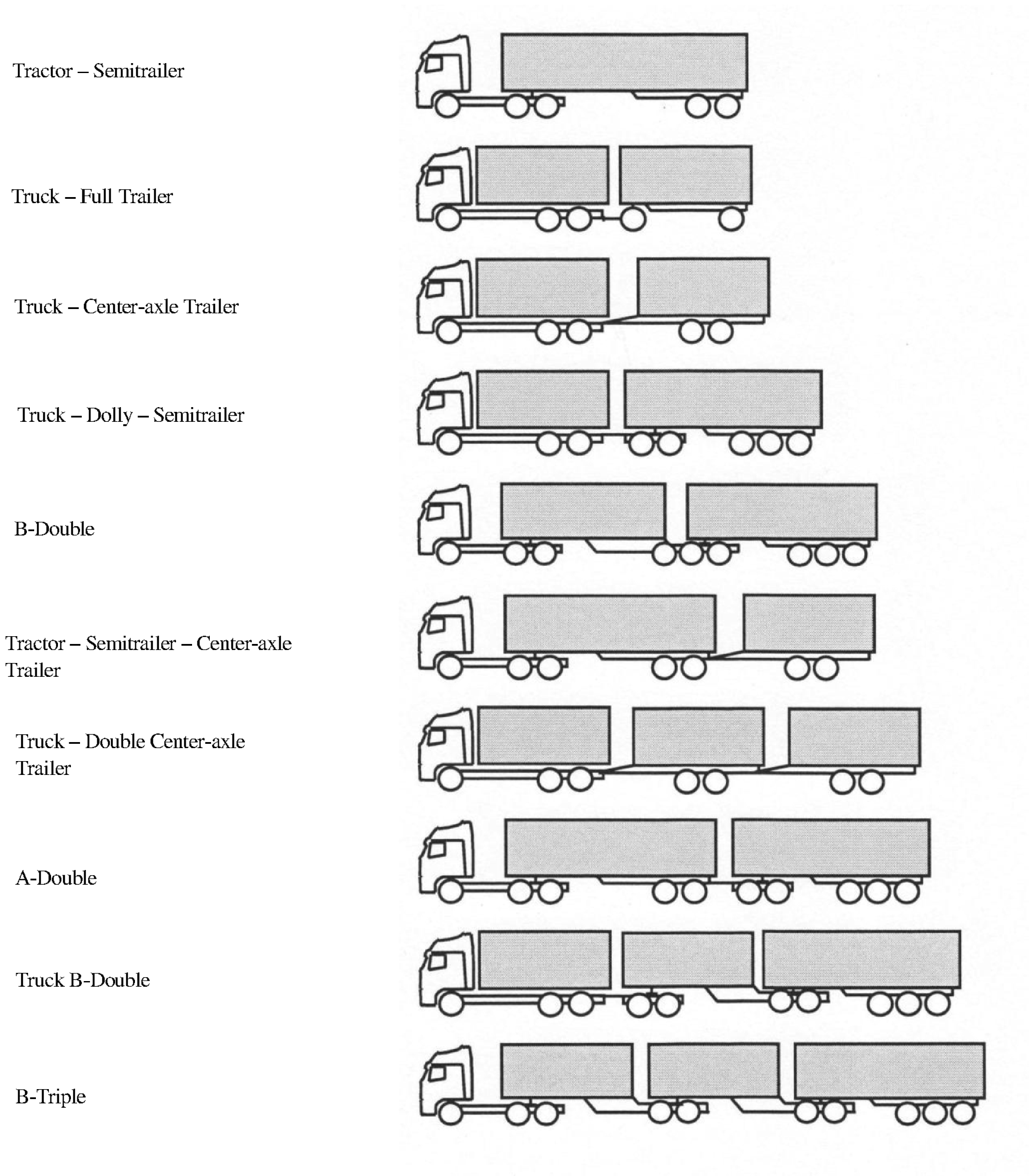

Figure 1.1: Different combinations of heavy vehicles.

1.2 Limitations and advantages

The long combinations vehicles, like the so called Scandinavian combination with total length of 25,25 meters, would lead to important advantages in terms of the reduction in fuel consumption, harmful emissions and road congestions.

By using longer combinations the fuel consumption and the associated emission are increased per vehicle. Nevertheless, two Scandinavian combination can carry a load equivalent to three EU-standard trucks [2]. Therefore, since the number of the vehicles on the road are reduced, the total fuel consumptions and the associated emissions are reduced. Moreover, using longer vehicles combinations the road congestions are decreased.

However, there are extra concerns about the traffic safety of some long combinations. Therefore, there is a strong motivation, from both safety and financial aspects, to study heavy truck hazardous motions and how they can be prevented or mitigated.

One of the most hazardous motions of heavy trucks is lateral instability which is of more concern when associated with high number of towed units. Instability in the towed units could result in undesired behavior of the vehicle and result in dangerous traffic accidents. In particular, lateral instability is associated with 9% of the traffic accidents involving heavy vehicles [16]. This represents a substantial figure, when translated into the absolute number of accidents, that has motivated the study of yaw and lateral stability control in heavy vehicles.

Since the middle of 90's there have been extensive research interests in improving the lateral instability of long combinations of heavy vehicles. In this study we focus on the latter and present a control algorithm to improve the vehicle lateral dynamic performance.

1.3 Thesis Objectives

Various control methods have been investigated to preserve the lateral stability in heavy vehicles by means of integrated braking and/or active steering in the towed units of the combination [17],[18] and [19]. In this study we focus on the stabilization of the lateral dynamics in long combinations of heavy vehicles. The lateral stability in heavy vehicles are quantified by two ISO standards, i.e., the RearWard Amplification (RWA) and off-tracking [6].

RWA is defined as the ratio between the maximum values of the motion variables (e.g., yaw rates, lateral accelerations), at the rearmost and the first units, respectively, during a specific maneuver. Off-tracking is the lateral deviation of the rearmost axle from the path followed by the front axle of the first unit. In particular, our objective is to suppress via active steering the lateral instability and tail swings of the towed units.

In this thesis we consider a truck-dolly-semitrailer combination, shown in Figure 2.1, a Scandinavian combination with total length of 25,25 meter and maximum weight of 60 tons, with individual axle steering capabilities for the dolly and the semitrailer. We propose a Model Predictive Control (MPC) approach to steer the axles in the dolly and semitrailer units to reduce the yaw rates and lateral accelerations RWA in two last units and also off-tracking of the vehicle rearmost unit.

Model predictive control is an effective approach to multivariable control problems with constraints. In MPC, a model of the plant is used to predict the future evolution of the system over a finite time horizon (i.e., the prediction horizon). Based on this prediction, at each time step a performance index is optimized under operating constraints with respect to a sequence of future input moves in order to best follow a given reference trajectory. The first of such optimal moves is the control action applied to the plant. At next time, a new optimization is solved for new system states over a shifted prediction horizon.

Next, we present the simulation scenarios at high speed, i.e., 80 kph, single lane change and double lane change maneuvers, where instability occurs.

The thesis is structured as follows. In Chapter 2 we present the vehicle model of the long combination considered in this thesis work. In Chapter 3, we state the vehicle dynamic control problem which is then formulated as an MPC problem. Simulation results using a high fidelity nonlinear vehicle model and also the experimental results obtained from real testing of the designed MPC controller on the vehicle are presented and analyzed in Chapter 4. Finally in Chapter 5, we close this manuscript and outline future works of the subject.

Chapter 2

Vehicle Model

In this chapter we derive mathematical models describing the vehicle yaw and lateral motion as function of the steering commands by using the basic equations of motion.

Basically, a vehicle model can be divided in two parts; tire model and chassis model [3]. Tire models are of crucial importance for dynamic behavior of the road vehicles. The basic forces that cause vehicle to move are generated by interaction of the tire and the surface of the road [14]. However, the tire models are complicated due to the tire complex nonlinear characteristics.

A chassis model determines the vehicle states and describes the motion of the vehicle based on the road forces acting on the vehicle, calculated by tire model [3]. Among the chassis models, the bicycle models are the simplest ones.

In this chapter we present a simplified long vehicle combination model for control design purposes. However, we will use a high fidelity vehicle model, whose parameters have been identified based on experimental data, for the simulation results presented in Section 4.3.1 .

2.1 Nonlinear Vehicle model

In this research we consider a truck-dolly-semitrailer combination in which all axles of the dolly and semitrailer can be steered. The combination is sketched in Figure 2.1. The vehicle combination consists of three vehicle units, each modeled as a rigid body. Two one degree-of-freedom frictionless cylindrical joints connect the three units. The dolly and the semitrailer have

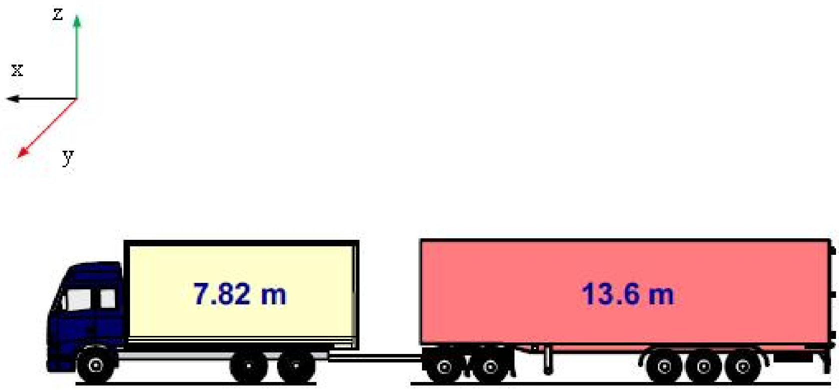

Figure 2.1: Truck - Dolly - Semitrailer.

two and three steering axles, respectively.

Consider Figure 2.1, by applying Newton's second law to center of gravity for each unit, the lateral, and yaw motions are described by the following set of equations:

$$m_i \dot{v_{y_i}} = \Sigma F_{y_i}, \tag{2.1a}$$
$$I_{z_i} \ddot{\psi}_i = \Sigma M_{z_i}. \qquad i = 1, ..., 3 \tag{2.1b}$$

Where $\ddot{\psi}_i$ is the angular acceleration and M_{zi} is angular momentum around z-axis for unit i.

The longitudinal dynamics are excluded in this model by assuming zero longitudinal forces and constant longitudinal velocity ($\ddot{x} = 0$). This will make the vehicle model easier to analyze for control design purposes. This nonlinear model will be further developed in next section by using bicycle model.

2.1.1 Bicycle model

In order to develop a simplified model of motion for the vehicle considered in this thesis, we use a bicycle model. In the bicycle model it is assumed that

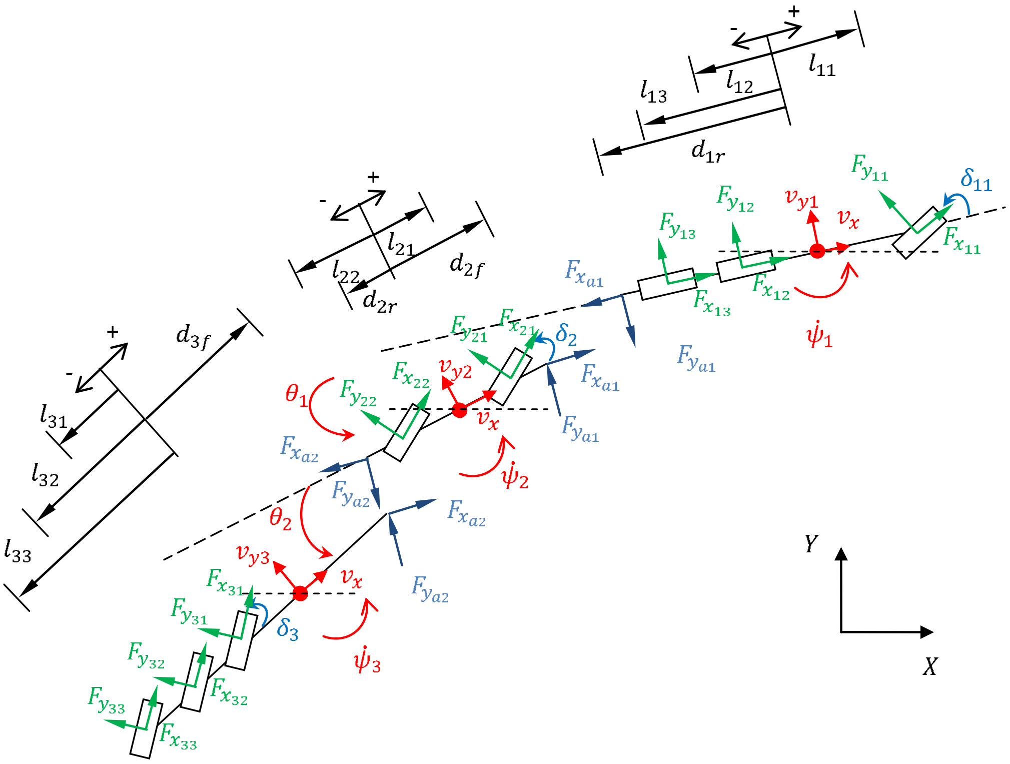

Figure 2.2: Bicycle model for combination of Truck-Dolly-Semitrailer.

the vehicle is perfectly symmetric with respect to its longitudinal axis so that two sides of the vehicle are identical. The bicycle model used in this study is depicted in Figure 2.1. In the proposed bicycle model we consider constant velocity maneuvers, i.e., $v_x = constant$. The union of the equations of motion for each unit, is an 8-order nonlinear dynamical model with 2 inputs [3].

In Figure 2.2 $F_{x_{ij}}$ and $F_{y_{ij}}$ are the lateral (or cornering) and longitudinal tire forces, respectively, acting on axle $j \in \{f, m, r\}$ of $i - th$ unit of the combination. Note that for the dolly we consider $j \in \{f, r\}$, since dolly have two steering axles.

$$F_{y_{ij}} = f_y(\alpha_{ij}, s_{ij}, \mu_{ij}, F_{z_{ij}}), \tag{2.2a}$$
$$F_{x_{ij}} = f_x(\alpha_{ij}, s_{ij}, \mu_{ij}, F_{z_{ij}}). \tag{2.2b}$$

According to equation (2.2) the tire forces depend on the tire slip angle α_{ij}, the slip ratio s_{ij}, road friction coefficient μ_{ij} and the tire normal force $F_{z_{ij}}$. tire slip angle α_{ij} is defined as the angle between the wheel velocity vector, v_j, and the direction of the wheel, as in Figure 2.3. The slip ratio s_{ij}

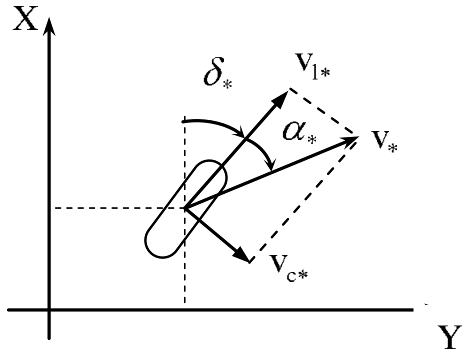

Figure 2.3: Side slip angle.

is defined as follows: [15]

$$s_{ij} = \begin{cases} \dfrac{r_\omega \omega_{ij} - v_x}{v_x}, & \text{if } v_x > r_\omega \omega_{ij},\ v_x \neq 0,\ \text{for braking} \\ \\ \dfrac{r_\omega \omega_{ij} - v_x}{r_\omega \omega_{ij}}, & \text{if } v_x < r_\omega \omega_{ij},\ r_\omega \omega_{ij} \neq 0,\ \text{for driving} \end{cases} \tag{2.3}$$

Due to the nonlinearities in the tire characteristics, the equations of motion represent a nonlinear vehicle model. This motivates the development of a linear version of the presented vehicle model for control design purposes.

2.2 Linear Parameter Varying (LPV) Vehicle model Based on Linear Tire Model and Small Angle Approximation

Two linear models of the vehicle will be introduced in this section. The main difference of these two linear models is the definition of the state spaces. The first model is the standard vehicle model, which is derived by the Newtonian method in Section 2.2.1. We will use this linear model, next in Section 3.1.1, to derive the yaw rates reference signals, i.e., as reference models. In the second model presented in Section 2.2.2, we use the Lagrange method to develop the vehicle model. The latter enables us to access the articulation angles, θ_1 and θ_2 for control design purposes. We will use this linear model, in Section 3.3, as the prediction model in MPC algorithms. These two models are developed based on the assumptions of linear tire characteristics and small angle approximation. In particular, the longitudinal and lateral tire forces are approximated as linear functions of longitudinal slip and the tire slip angle, respectively [3, 4]:

$$F_{x_{ij}} = C_{lij} s_{ij}, \tag{2.4a}$$

$$F_{y_{ij}} = -C_{cij}(\beta_i + \frac{\dot{\psi} l_{ij}}{\dot{x}}). \tag{2.4b}$$

where C_{lij} are the *longitudinal stiffness coefficients* and C_{cij} are the *cornering stiffness coefficients* of the $j-th$ axle of the $i-th$ unit.

The longitudinal dynamics are neglected and the longitudinal velocity $\dot{x}$ appears as a constant parameter. Hence, both linear models will be Linear Parameter Varying (LPV) vehicle models.

2.2.1 Linear Model Derived by Newtonian Method

The first linear model is obtained by using Newtonian method 2.2.1. The equations of motion for each unit of the combination, according to Figure 2.2 and based on the assumptions of linear tire model, small angle approximation and constant longitudinal velocity are [3].

$$m_1 \dot{x}(\dot{\beta}_1 + \dot{\psi}_1) = \Sigma F_y = F_{\beta_1}\beta_1 + F_{\dot{\psi}_1}\dot{\psi}_1 + C_{11}\delta_{11} - F_{ya_1}, \tag{2.5a}$$

$$I_{z_1}\ddot{\psi}_1 = \Sigma M_z = M_{\beta_1}\beta_1 + M_{\dot{\psi}_1}\dot{\psi}_1 + C_{11} l_{11}\delta_{11} - F_{ya_1} d_{1r}, \tag{2.5b}$$

$$m_2 \dot{x}(\dot{\beta}_2 + \dot{\psi}_2) = \Sigma F_y = F_{\beta_2}\beta_2 + F_{\dot{\psi}_2}\dot{\psi}_2 + F_{ya_1} - F_{ya_2} - F_{\beta_2}\delta_2, \tag{2.6a}$$

$$I_{z_2}\ddot{\psi}_2 = \Sigma M_z = M_{\beta_2}\beta_2 + M_{\dot{\psi}_2}\dot{\psi}_2 + F_{ya_1} d_{2f} - F_{ya_2} d_{2r} - M_{\beta_2}\delta_2, \tag{2.6b}$$

$$m_3\dot{x}(\dot{\beta}_3+\dot{\psi}_3)=\Sigma F_y=F_{\beta_3}\beta_3+F_{\dot{\psi}_3}\dot{\psi}_3+F_{ya_2}-F_{\beta_3}\delta_3, \tag{2.7a}$$

$$I_{z_3}\ddot{\psi}_3=\Sigma M_z=M_{\beta_3}\beta_2+M_{\dot{\psi}_3}\dot{\psi}_3+F_{ya_2}d_{3f}-M_{\beta_3}\delta_3. \tag{2.7b}$$

where,

$$F_{\beta_i}=-\sum_j C_{ij}, \tag{2.8a}$$

$$F_{\dot{\psi}_i}=-\sum_j \frac{C_{ij}l_{ij}}{\dot{x}}, \tag{2.8b}$$

$$M_{\beta_i}=-\sum_j C_{ij}l_{ij}, \tag{2.8c}$$

$$M_{\dot{\psi}_i}=-\sum_j \frac{C_{ij}l_{ij}^2}{\dot{x}}. \tag{2.8d}$$

Equations (2.5) correspond to the truck motion and equations (2.6) and (2.7) represent the dolly and the semitrailer motions, respectively.

Combining the equations (2.5) - (2.7) and (2.8) together will result in:

$$\begin{aligned}&d_{1r}m_1\dot{x}(\dot{\beta}_1+\dot{\psi}_1)-I_{z_1}\ddot{\psi}_1=(F_{\beta_1}d_{1r}-M_{\beta_1})\beta_1+(F_{\dot{\psi}_1}d_{1r}-M_{\dot{\psi}_1})\dot{\psi}_1\\&+C_{11}(d_{1r}-l_{11})\delta_{11},\end{aligned} \tag{2.9a}$$

$$\begin{aligned}&d_{3f}m_3\dot{x}(\dot{\beta}_3+\dot{\psi}_3)-I_{z_3}\ddot{\psi}_3=(F_{\beta_3}d_{3f}-M_{\beta_3})\beta_3+(F_{\dot{\psi}_3}d_{3f}-M_{\dot{\psi}_3})\dot{\psi}_3\\&(M_{\beta_3}-F_{\beta_3}d_{3f})\delta_3,\end{aligned} \tag{2.9b}$$

$$\begin{aligned}&m_1\dot{x}(\dot{\beta}_1+\dot{\psi}_1)+m_2\dot{x}(\dot{\beta}_2+\dot{\psi}_2)+m_3\dot{x}(\dot{\beta}_3+\dot{\psi}_3)=F_{\beta_1}\beta_1+F_{\dot{\psi}_1}\dot{\psi}_1\\&+C_{11}\delta 11+F_{\beta_2}\beta_2+F_{\dot{\psi}_2}\dot{\psi}_2+F_{\beta_3}\beta_3+F_{\dot{\psi}_3}\dot{\psi}_3-F_{\beta_2}\delta_2-F_{\beta_3}\delta_3,\end{aligned} \tag{2.9c}$$

$$\begin{aligned}&d_{2f}m_1\dot{x}(\dot{\beta}_1+\dot{\psi}_1)-I_{z_2}\ddot{\psi}_2+d_{2r}m_3\dot{x}(\dot{\beta}_3+\dot{\psi}_3)=F_{\beta_1}d_{2f}\beta_1+F_{\dot{\psi}_1}d_{2f}\dot{\psi}_1\\&+C_{11}d_{2f}\delta_{11}+M_{\beta_2}\beta_2+M_{\dot{\psi}_2}\dot{\psi}_2+F_{\beta_3}d_{2r}\beta_3+F_{\dot{\psi}_3}d_{2r}\dot{\psi}_3-M_{\beta_2}\delta_2\\&-F_{\beta_3}d_{2r}\delta_3.\end{aligned} \tag{2.9d}$$

The kinematical constraint (in lateral direction; v_x is constant) at the articulation joints are given by equations (2.10):

$$\dot{\beta}_2 = \dot{\beta}_1 + \frac{d_{1r}}{\dot{x}}\ddot{\psi}_1 - \frac{d_{2f}}{\dot{x}}\ddot{\psi}_2 + \dot{\psi}_1 - \dot{\psi}_2, \tag{2.10a}$$

$$\dot{\beta}_3 = \dot{\beta}_2 + \frac{d_{2r}}{\dot{x}}\ddot{\psi}_2 - \frac{d_{3f}}{\dot{x}}\ddot{\psi}_3 + \dot{\psi}_2 - \dot{\psi}_3. \tag{2.10b}$$

The equations presented in (2.9a)-(2.9d) along with equations (2.10a) and (2.10b) represent the linear model derived by Newtonian method. Putting the proposed linear model in the matrix form gives the following state space model of the vehicle:

$$\dot{x}_s(t) = M_s^{-1}(p)A_s(p)x_s(t) + M_s^{-1}(p)B_s(p)u(t) + M_s^{-1}(p)E_s(p)d(t) \tag{2.11}$$

where x_s, u and d are defined as in (2.12)-(2.14).For control design purposes, the steering angle at the front axle of the truck is considered as disturbance d according to (2.14). p is the longitudinal velocity of the vehicle which appears as a constant parameter.

$$x_s = \left[\beta_1,\ \dot{\psi}_1,\ \beta_2,\ \dot{\psi}_2,\ \beta_3,\ \dot{\psi}_3\right], \tag{2.12}$$

$$u = [\delta_2, \delta_3], \tag{2.13}$$

$$d = [\delta_{11}] \tag{2.14}$$

Remark 1 *In order to simplify both the model and the control design, it is assumed that the steering angles for each of the axles on both the dolly and semitrailer are the same, and are represented by the "lumped" steering angles* δ_2 *and* δ_3*, respectively.*

The parameter varying matrices $M_s(p)$, $A_s(p)$, $B_s(p)$ and $E_s(p)$ introduced in (2.11) are given in A.1.

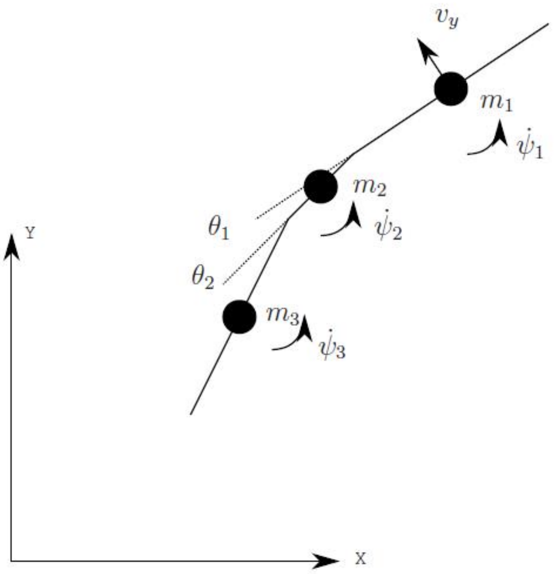

Figure 2.4: Single Track Model for the combination.

2.2.2 Linear model developed through the Lagrange method

In this section the Lagrange's method is used to develop a linear vehicle model. The Lagrange's method, in conjunction with a choice of independent configuration coordinates allows the dynamics of the system to be derived relatively easy. That is, based on the Lagrange method, we only require the external forces acting on the vehicle, so that the determination of internal forces occurring at the joints are not required [5].

The state vector in this model is defined as follows:

$$x_b = \left[v_{y_1},\ \dot{\psi}_1,\ \theta_1,\ \theta_2,\ \dot{\theta}_1,\ \dot{\theta}_2\right]^T, \tag{2.15}$$

where v_{y_1} is the lateral velocity of the truck, $\dot{\psi}_1$ is the yaw rate of the truck, θ_1 and θ_2 are the first and second articulation angles, respectively and $\dot{\theta}_1$ and $\dot{\theta}_2$ are the articulation angle derivatives, respectively.

To form the Lagrangian, the kinetic energies of the combination are determined individually and summed together. The kinetic energy of each unit T_1,T_2 and T_3 depend on the states as follows [5]:

$$\begin{aligned}
T_1 &= T_1(v_x, v_{y_1}, \dot{\psi}_1), \\
T_2 &= T_2(v_x, v_{y_1}, \dot{\psi}_1, \theta_1, \dot{\theta}_1), \\
T_3 &= T_3(v_x, v_{y_1}, \dot{\psi}_1, \theta_1, \dot{\theta}_1, \theta_2, \dot{\theta}_2).
\end{aligned} \tag{2.16}$$

Dependency of kinetic energies (2.16) to the chosen states (2.15) stems from the relations between the yaw rates of the units and articulation angle derivatives [5]:

$$\begin{aligned}
\dot{\psi}_2 &= \dot{\psi}_1 + \dot{\theta}_1 \\
\dot{\psi}_3 &= \dot{\psi}_2 + \dot{\theta}_2 \\
&= \dot{\psi}_1 + \dot{\theta}_1 + \dot{\theta}_2
\end{aligned} \tag{2.17}$$

The Lagrangian can then be formed as:

$$L = T_1 + T_2 + T_3. \tag{2.18}$$

Note that according to (2.16), the kinetic energy of each unit of the combination depends on the longitudinal velocity v_x. Nevertheless, since the constant longitudinal velocity is assumed in this study, v_x is considered as a constant value and appears only as a parameter in (2.16).

Using kinetic energies in (2.16), the equations of motion are then obtained from Lagrange's equations:

$$\frac{d}{dt}\frac{\partial L}{\partial \dot{q}_i} + \frac{\partial L}{\partial q_i} = Q_i \tag{2.19}$$

where q_i are the generalized coordinates and Q_i the generalized external forces.

Since the choice of states in (2.15) does not correspond to a set of inertial coordinates, it is required to define a set of inertial coordinates and map the chosen (non-inertial) states (2.15) into inertial coordinates.

An appropriate choice of inertial coordinates are the position of the truck CoG, X_1 and Y_1 and its yaw angle in an inertial frame, ψ_1 and the articulation angles θ_1 and θ_2, (2.20).

$$q = [X_1,\ Y_1,\ \psi_1,\ \theta_1,\ \theta_2], \tag{2.20}$$

The Lagrange equations may then be transformed appropriately by using the following dynamic mapping between the state vector and the inertial coordinates:

$$
\begin{aligned}
v_{x_1} &= \dot{X}_1 cos(\psi_1) + \dot{Y}_1 sin(\psi_1), \\
v_{y_1} &= \dot{X}_1 sin(\psi_1) + \dot{Y}_1 cos(\psi_1).
\end{aligned}
\tag{2.21}
$$

The generalized external forces Q_i in (2.19) depend on the lateral tire forces which are assumed to be a linear function of tire slip angles (see equation (2.4b). Note that the longitudinal tire forces are assumed to be zero.

Assuming small angle approximation for steering and articulation angles, Lagrange equations can be linearized around a constant-velocity and zero steering angle. The lateral velocities for the dolly and semitrailer are approximated as the sums of lateral velocity of the truck and the linear velocities of the dolly and semitrailer centers of mass about the truck center of mass due to the respective rotations [5].

Finally, the derived linear parameter varying vehicle model can be described by the following compact system of linear differential equations:

$$
\dot{x}_b(t) = M_b^{-1}(p)A_s(p)x_b(t) + M_b^{-1}(p)B_b(p)u(t) + M_b^{-1}(p)E_b(p)d(t) \tag{2.22}
$$

where the state vector X_b is given as in (2.15) and the input vector u and disturbance d are defined as (2.13) and (2.14), respectively.

The parameter varying matrices $M_b(p)$, $A_b(p)$, $B_b(p)$ and $E_b(p)$ in which p is the longitudinal velocity of the vehicle v_x, are reported in A.2.

Chapter 3

Control Design

In this chapter, the vehicle dynamic control problem for this study is discussed and the control objectives are presented.

3.1 Vehicle Dynamic Control problem

The yaw rate frequency responses of the truck, dolly and semitrailer for the passive case, i.e., $\delta_2 = \delta_2 = 0$ are illustrated in Figure 3.1 for a longitudinal velocity of 80 kph. We observe that the yaw rates of the dolly and semitrailer are amplified at the frequency about 0.4 Hz, compared to the truck yaw rate. Namely, the yaw rate RWA for the dolly and semitrailer are higher than 1, when the frequency of the truck steering angle δ_{11} is around 0.4 Hz. Such yaw rate amplification at two last units of the combination are not desired and should be prevented.

The control objective is to decrease the yaw rate RWA of two last units of the combination below one, i.e., $RWA \leq 1$. This can be achieved via active steering the axles at the dolly and the semitrailer. Moreover, the steering wheel angle of the front axle of the truck, driver input, is considered as a disturbance to the system.

3.1.1 Reference Generation

In order to reduce the yaw rate RWA at dolly and semitrailer, we formulate an output tracking problem. The yaw rate reference signals, $\dot{\psi}_{2_{ref}}(t)$ and $\dot{\psi}_{3_{ref}}(t)$, for the dolly and the semitrailer, respectively, are generated as the

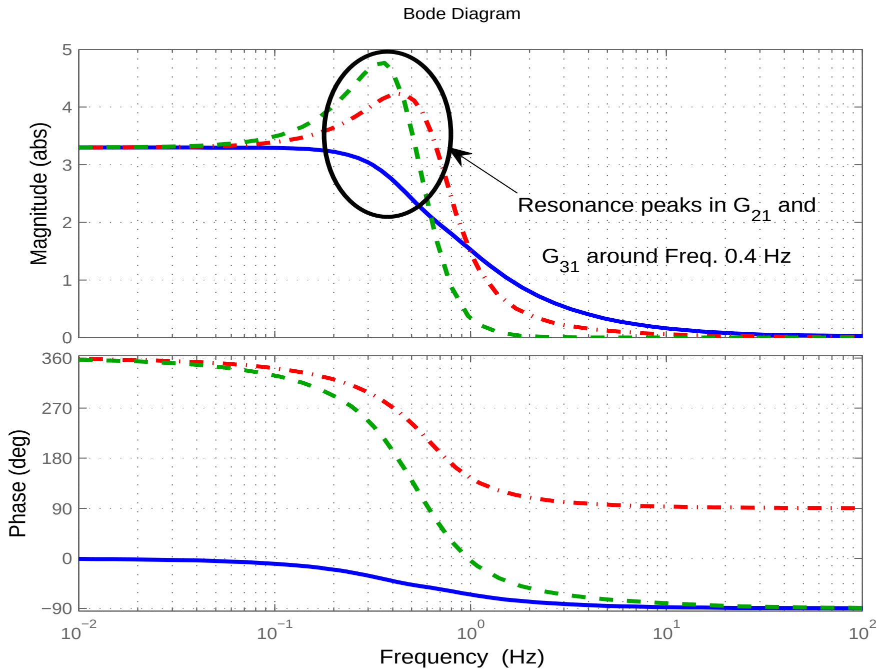

Figure 3.1: Frequency responses of the truck (solid line), dolly (dash-dotted line) and semitrailer (dashed line) yaw rates G_{11}, G_{21} and G_{31} respectively for the passive vehicle, i.e., $\delta_2 = \delta_3 = 0$.

outputs of the following transfer functions:

$$G_{21_{ref}}(s) = \frac{\dot{\Psi}_{2_{ref}}(s)}{\Delta_{11}(s)} \tag{3.1a}$$

$$G_{31_{ref}}(s) = \frac{\dot{\Psi}_{3_{ref}}(s)}{\Delta_{11}(s)}, \tag{3.1b}$$

where $\dot{\Psi}_{2_{ref}}(s)$, $\dot{\Psi}_{3_{ref}}(s)$ and $\Delta_{11}(s)$ are the Laplace transforms of the yaw rate reference signals, $\dot{\psi}_{2_{ref}}$ and $\dot{\psi}_{3_{ref}}$, and front steering angle of the truck, δ_{11}, respectively. The transfer functions $G_{21_{ref}}(s)$ and $G_{31_{ref}}(s)$ have to be designed such that the yaw rate RWA, calculated for $\dot{\psi}_{2_{ref}}$ and $\dot{\psi}_{3_{ref}}$, are less than 1.

To define the reference signals, primarily the yaw rate frequency responses of each unit to the truck steering are studied. These transfer functions are derived from the linear model described in the previous section. Next, we de-

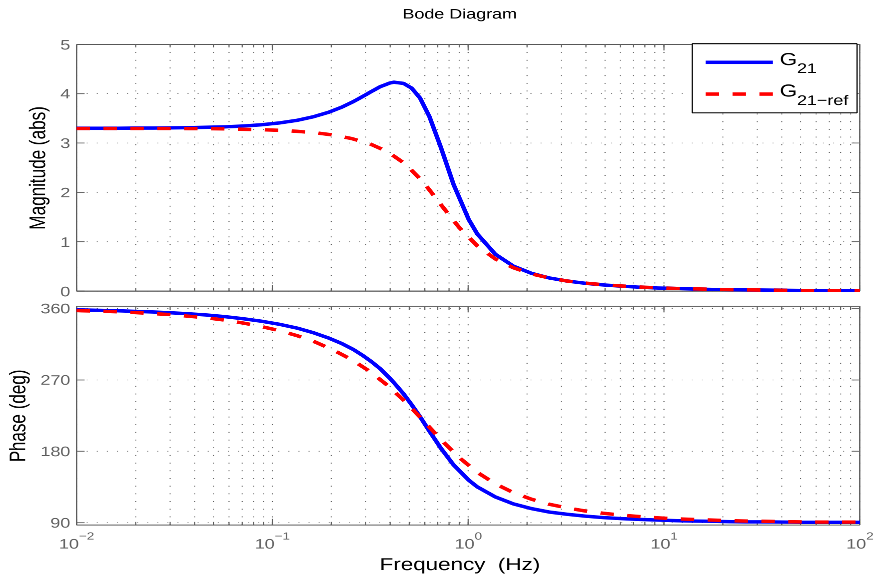

Figure 3.2: Frequency response of $G21_{ref}$ together with G_{21}.

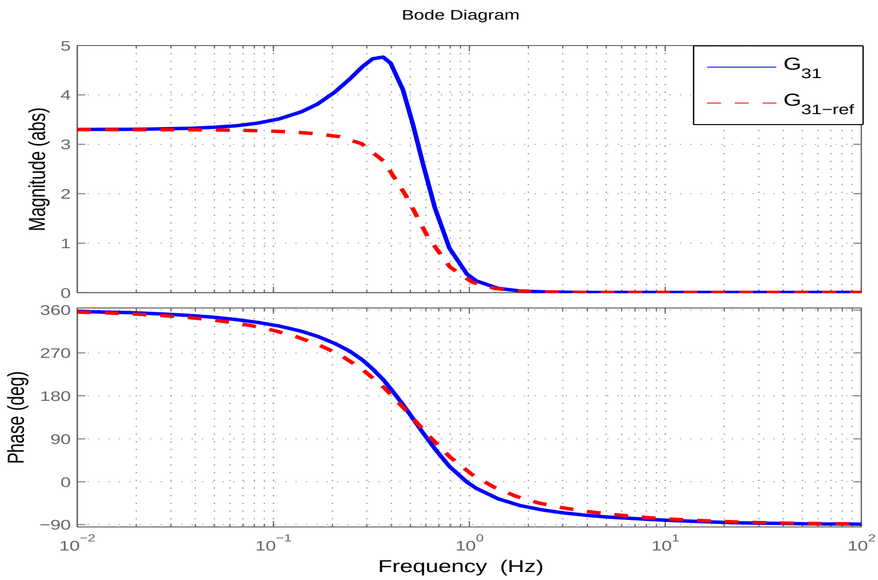

Figure 3.3: Frequency response of $G31_{ref}$ together with G_{31}.

sign the yaw rate references, $G21_{ref}$ and $G31_{ref}$, such that they have the same magnitude as the truck yaw rate frequency response, G_{11}, and the resonance peaks, highlighted in Figure 3.1, are eliminated. This is done by shaping $G21_{ref}$ and $G31_{ref}$. However, the phase responses of the reference models must be kept as close as possible to responses of the dolly and semitrailer in the passive case. Such design of the reference models maintains natural time lags between the yaw rate responses of the three units.

The frequency responses of the reference transfer functions, $G_{21_{ref}}$ and $G_{31_{ref}}$, together with frequency responses for the passive case, G_{21} and G_{31} are shown in Figure 3.2 and 3.3. The yaw rate reference signals generated for the dolly and the semitrailer through $G_{21_{ref}}$ and $G_{31_{ref}}$, are used in a model predictive control algorithm presented next in section 3.3.

3.1.2 System Constraints

Due to the physical limitations on the steering actuators, the control inputs (δ_2 and δ_3) i.e., the steer angles and steering rates at the dolly and the semitrailer are subject to the following constraints:

$$\delta_{min} \leq \delta_i \leq \delta_{max}, \tag{3.2a}$$

$$\dot{\delta}_{min} \leq \dot{\delta}_i \leq \dot{\delta}_{max}, \qquad i = 2,\ 3 \tag{3.2b}$$

3.2 MPC formulation

Model predictive control (MPC), also referred to as moving horizon control or receding horizon control, has become an attractive feedback strategy. For MIMO processes with constraints, MPC can offer substantial performance improvement compared with traditional control strategies [7]. Its ability to deal with large multivariable constrained control problems, has made MPC quite popular in industry, over the past 30 years [21]. Firstly it was widely used in Petrochemical industry [8], [9]. Currently with its development, MPC applications have been increasing in Automotive and Aerospace industries.

Consider the following discrete-time system:

$$\dot{x} = f(x, u, t) \tag{3.3}$$

where f is the state update function, x is the state vector and u is the control input. System (3.3) is subject to the following state and input constraints:

$$x \in X, \tag{3.4a}$$
$$u \in U, \tag{3.4b}$$

where X and U are the bounds on the state vector and control input, respectively.

We consider the cost function J defined as follows [4]:

$$J_N(x(k), U(k)) = \sum_{k=t}^{t+N-1} l(x(k), u(k)) + P(x(t+N)), \tag{3.5}$$

where $U(t) = [u(t), ..., u(t+N-1)]$ is a sequence of inputs over the time horizon N, $x(k)$ for $k = t, ..., t+N$ is the state trajectory obtained by applying the control sequence $U(t)$ to the system (3.3), $l(.,.)$ is the stage cost and $P(.)$ is the terminal cost.

To formulate a model predictive control problem we consider the cost function $J_N(x(t), U(t))$ in (3.5) at each sampling time t. We assume that a state measurement $x(t)$ is available and solve the following optimization problem:

$$\min_{U_t, x_{t+1}, \ldots, x_{t+N}} \quad J(x_t, U_t)$$
$$\text{subj. to}$$
$$x_{k+1} = f(x_k, u_k), \qquad k = t, \ldots, N-1 \tag{3.6a}$$
$$x_k \in X, \qquad k = t+1, \ldots, t+N-1 \tag{3.6b}$$
$$u_k \in U, \qquad k = t, \ldots, t+N-1 \tag{3.6c}$$
$$x_k = x(t) \tag{3.6d}$$

We denote by $U_t^* = [u_t^*, u_{t+1}^*, ..., u_{t+N-1}^*]$ as the solution of the optimization problem (3.6) at time t. The first sample of U_t^* is selected as the control action at time t and applied to the plant:

$$u(x(t)) = u_t^* \tag{3.7}$$

At the next the sampling time, the optimization problem (3.6) is solved over a shifted horizon.

3.3 MPC approach to lateral and yaw vehicle dynamics control

In this section we present an MPC algorithm to solve the yaw rate control problem based on the linear model of the vehicle introduced in Chapter 2. The linear model used to predict the future evolution of the system is the one introduced in Section 2.2.2. This choice of the linear model results in a state vector that easily measured. Given the state space model 2.22 at time t, the following discrete-time linear time varying (LTV) model of the system is obtained:

$$x_{k+1} = A_t x_k + B_t u_k + E_t d_k,$$

$$y_k = C_t x_k + D_t u_k. \tag{3.8}$$

where the matrices A_t, B_t, C_t, D_t and E_t are the matrices introduced in (2.22).

Based on the discrete-time LTV model (3.8), we consider the following prediction model:

$$\tilde{x}_{k+1,t} = \tilde{A}_t \tilde{x}_{k,t} + \tilde{B}_t \Delta u_{k,t} + \tilde{E}_t \tilde{d}_{k,t},$$

$$y_{k,t} = \tilde{C}_t \tilde{x}_{k,t} + \tilde{D}_t \Delta u_{k,t}. \tag{3.9}$$

where,

$$\tilde{A}_t = \begin{pmatrix} A_t & B_t \\ 0_{m\times n} & I_m \end{pmatrix}, \tilde{B}_t = \begin{pmatrix} B_t \\ I_m \end{pmatrix}, \tilde{E}_t = E_t \tag{3.10a}$$

$$\tilde{C}_t = \begin{pmatrix} C_t & D_t \end{pmatrix}, \tilde{D}_t = D_t \tag{3.10b}$$

$$\tilde{x}_{k,t} = \begin{pmatrix} x_{k,t} \\ u_{k-1,t} \end{pmatrix}, \tilde{d}_{k,t} = d_{k,t} \tag{3.10c}$$

$$\tag{3.10d}$$

$0_{m\times n}$ is a matrix with nm zeros 0_m is a column vector of m zeros, I_m is an identity matrix of dimension m, $\Delta u_{k,t} = u_{k,t} - u_{k-1,t}$ and $u_{t-1,t} = u_{t-1}$. Note that inclusion of $\Delta u(k)$ enables us to have the input variations as the optimization variable in MPC problem.

Consider the following objective function:

$$
\begin{aligned}
J(x(t), u(t-1), \Delta U(t)) = \; & \sum_{i=1}^{H_p} \|y_{tr}(t+i|t) - y_{ref}(t+i|t)\|_Q^2 \\
& + \sum_{i=0}^{H_u-1} \|\Delta u(t+i|t)\|_R^2 + \sum_{i=0}^{H_u-1} \|u(t+i|t)\|_S^2 .
\end{aligned}
\tag{3.11}
$$

where H_p and H_u are the prediction and control horizons respectively, $y_{ref}(t+i)$ with $i = 1, ..., H_p$, is the output reference signal generated through the reference models (3.1), $Q \in \mathbb{R}^{p_y\times p_y}$ and $S, R \in \mathbb{R}^{m\times m}$ are weighting matrices. The term $y_{tr}(t+i|t)$ represents the prediction at the time instant $t+i$ given the measurements at time t.

Given the states of the system at time k as initial states $x(k)$, we solve the following optimization problem to achieve the sequence of control actions $u^*(k+i)$ for $i = 0, ..., H_u - 1$ at time k:

$$
\begin{aligned}
\min_{\Delta U_t} \quad & J(x_t, u_{t-1}, \Delta U_t) \\
\text{subj. to} \quad & \\
& x_{k+1,t} = A_t x_{k,t} + B_t u_{k,t} + E_t d_{k,t}, && (3.12a)\\
& y_{k,t} = h(x_{k,t}) && (3.12b)\\
& \qquad k = t, \ldots, t+H_p-1 \\
& x_{t,t} = x(t), && (3.12c)\\
& u_{k,t} = u_{k-1,t} + \Delta u_{k,t}, && (3.12d)\\
& u_{f,min} \le u_{k,t} \le u_{f,max}, && (3.12e)\\
& \Delta u_{f,min} \le \Delta u_{k,t} \le \Delta u_{f,max}, && (3.12f)\\
& \qquad k = t, \ldots, t+H_c-1 \\
& u_{t-1,t} = u(t-1), && (3.12g)\\
& \Delta u_{k,t} = 0, \quad k = t+H_c, \ldots, t+H_p && (3.12h)
\end{aligned}
$$

where the equations (3.12a) and (3.12b) show the linear discrete time model of the system at time t. The bounds in the inequalities (3.12e) and (3.12f), are derived from the constraints (3.2a) and (3.2b) set by the steering actuators. Equations (3.12c) and (3.12g), initialize state and input vectors, respectively. The input rates for the prediction instants above $H_u - 1$ are defined by (3.12h).

In order to reduce the computational complexities, the cost function J is optimized only over the sequence of the input changes $\Delta u_{k,t}$, with $k = t, ..., t + H_u - 1$. The control inputs are then held over the time interval $k = t + H_u, ..., t + H_p$.

We denote the $\Delta U_t^* \triangleq [\Delta u_{t,t}^*, \ldots, \Delta u_{t+H_u-1,t}^*]$ as the solution of the optimization problem 3.12 at time t for current states of the system $x(t)$ and the previous input $u(t-1)$. Finally, the control action at time t is computed as below:

$$u(t, \xi(t)) = u(t-1) + \Delta u_{t,t}^*(t, \xi(t)). \tag{3.13}$$

At next time instant, $t + 1$, the optimization problem 3.12 is formulated and solve over a shifted horizon.

Remark 2 *The cost function 3.11 is quadratic and since the constraints 3.12a and 3.12b are linear, the optimization problem 3.12 is convex. Due to the quadratic form of the cost function and convexity of the constraints, we use quadratic programming (QP) optimization techniques to solve the proposed MPC problem.*

Chapter 4

Simulation and Experimental Results

In this chapter we present and discuss the results obtained from the simulations and experimental testing of the designed MPC controller. Moreover, the steps to implement the designed MPC controller on a vehicle for experimental testing is described.

4.1 Testing Scenario

One of the most critical maneuvers causing the lateral instability, particularly in the case of long combinations of heavy vehicles is the lane change maneuver. In this research, we consider a single lane change maneuver performed at 80 Kph on a dry road. The maneuver is performed in open loop, i.e., a predefined steering profile is used (steering robot) at the truck.

4.2 Sampling Rate

Choice of the sampling rate for the presented MPC controller is of great importance. This parameter plays an important role in increasing the computational time in real time applications. The sampling period influences the size of the MPC problem. Therefore, the choice of the sampling rate determines the size of the optimization problem. The choice of the sampling rate should be done such that a stable discrete time linear model of the system is obtained.

v_x [kph]	System Poles	Fastest dynamic
80	$-1.4878 \pm 3.7844i$ $-2.5340 \pm 1.2985i$ $-1.2821 \pm 2.3952i$	$-2.5340 \pm 1.2985i$

Table 4.1: Poles of the syetem 2.22.

In order to obtain a stable discrete time linear model at 80 Kph we use the criterion introduced in [12] to attain a suitable sampling rate. According to this criterion, for a second-order system with the natural frequency ω_0 and damping ratio around $\zeta \approx 0.7$ the following expression is given:

$$\omega_0 T_s \approx 0.2 - 0.6 \tag{4.1}$$

where T_s is the sampling rate.

Consider the fastest dynamics of the system (2.22) reported in Table 4.1. We obtain the natural frequency of $\omega_0 = 2.8473$ and $\zeta \approx 0.78$. Therefore, using the criterion (4.1), a sampling rate of 0.07 sec is selected.

Remark 3 *The sampling rate of the presented MPC problem formulation is equal to the sampling rate used for the continuous time discretization of the vehicle model. The real-time testing of the controller showed that aforementioned sampling time for the designed MPC controller is a feasible choice in terms of computational complexity for solving optimization problem.*

The simulation step size to run the vehicle model in a closed loop with the MPC controller is the fixed step size of 0.01 sec. This sampling was selected according to the dynamics of the vehicle model, we refer to the non-linear vehicle model 2.1. However, the sampling time of the MPC controller, as explained before, is 0.07 sec meaning that the control command is hold constant for every 7 samples.

4.3 MPC Controllers

In this section we introduce two MPC controllers, designed according to the design procedure presented in Chapter 3. These two MPC controllers are described as follows:

- **Controller A**, This controller is designed to track the yaw rate references. Yaw rate references are generated, as explained in Section 3.1.1 and tracked by steering the dolly and semitrailer steered axles. However, as shown next in Section 4.3.1, this controller does not guarantee the alignment of the three units at the end of the single lane change maneuver.

- **Controller B**, This controller is designed to alleviate the aforementioned problem of the Controller A. In Controller B, both the yaw rates and articulation angles are tracked. The reference signals for the articulation angles are simply created by integrating and subtracting the yaw rate reference signals as given in (4.2).

$$\theta_{1_{ref}}(t) = \int \dot{\psi}_{2_{ref}}(t) - \dot{\psi}_{1_{ref}}(t) \tag{4.2a}$$

$$\theta_{2_{ref}}(t) = \int \dot{\psi}_{3_{ref}}(t) - \dot{\psi}_{2_{ref}}(t) \tag{4.2b}$$

The following tuning parameters for the designed controllers are used in simulations:

- sampling time: $T = 0.07$s.
- horizons: $H_p = 15$, $H_c = 1$, $H_u = 5$.
- bounds:
  - $\delta_{2_{\min}} = -5$ deg, $\delta_{2_{\max}} = 5$ deg,
    $\delta_{3_{\min}} = -5$ deg, $\delta_{3_{\max}} = 5$ deg.
  - $\Delta\delta_{2_{\min}} = -1$ deg, $\Delta\delta_{2_{\max}} = 1$ deg,
    $\Delta\delta_{3_{\min}} = -1$ deg, $\Delta\delta_{3_{\max}} = 1$ deg.

Controller A

- weighting matrices:
  - $Q \in \mathbb{R}^{2\times 2}$ with $Q_{11} = 0.55$, $Q_{22} = 0.72$, and
    $Q_{ij} = 0$ for $i \neq j$..

- $R \in \mathbb{R}^{2\times2}$ with $R_{11} = R_{22} = 36$, and $R_{ij} = 0$ for $i \neq j$.
- $S \in \mathbb{S}^{2\times2}$ with $S_{11} = S_{22} = 1$ and $S_{ij} = 0$ for $i \neq j$.

Controller B

- weighting matrices:
  - $Q \in \mathbb{R}^{4\times4}$ with $Q_{11} = 2,\ Q_{22} = 4,\ Q_{33} = 2,\ Q_{44} = 2$ and $Q_{ij} = 0$ for $i \neq j$..
  - $R \in \mathbb{R}^{2\times2}$ with $R_{11} = R_{22} = 3$ and $R_{ij} = 0$ for $i \neq j$.
  - $S \in \mathbb{S}^{2\times2}$ with $S_{11} = S_{22} = 10$ and $S_{ij} = 0$ for $i \neq j$.

Note that the upper and lower bounds on the steering angles at the dolly and semitrailer are selected considering the actual limitations on the steering and steering dynamics.

4.3.1 Simulation Results

Next we present and discuss the simulation results of two MPC controllers. The simulation results are obtained in Matlab R2007b. The proposed MPC controllers are developed using Simulink environment and by means of the built in blocks and some user defined C-coded S-functions. A high fidelity vehicle model whose parameters have been determined by experimental data is used to simulate the plant. We point out that all the simulations results presented in this section have been obtained by using a simulation model including sensors noises. Noises are modeled as zero mean measurement noises for which the variances have been identified based on experimental data as shown in Table 4.2.

Sensor	$\dot{\psi}_1$ $[\frac{rad}{sec}]$	$\dot{\psi}_2$ $[\frac{rad}{sec}]$	$\dot{\psi}_3$ $[\frac{rad}{sec}]$	a_{y_1} $[\frac{m}{sec^2}]$	a_{y_2} $[\frac{m}{sec^2}]$	a_{y_3} $[\frac{m}{sec^2}]$
Noise variance	0.0022^2	0.0011^2	0.0011^2	0.05^2	0.0131^2	0.0131^2

Table 4.2: Noise variances.

In Figure 4.1, the simulation results for the passive vehicle, i.e., dolly and semitrailer are not steered, are shown. We observe that the yaw rates at the dolly and semitrailer are amplified compared to the truck yaw rate when the steering profile in Figure 4.2 is implemented. Moreover as shown in Figures 4.3 and 4.4, the lateral accelerations and side slip angles at the dolly and semitrailer are considerably amplified in comparison with the truck. In order to better evaluate the vehicle responses in proposed maneuver, the yaw rate, lateral acceleration and side slip angle RWAs values of the towed units are reported in the first column of Table 4.3.

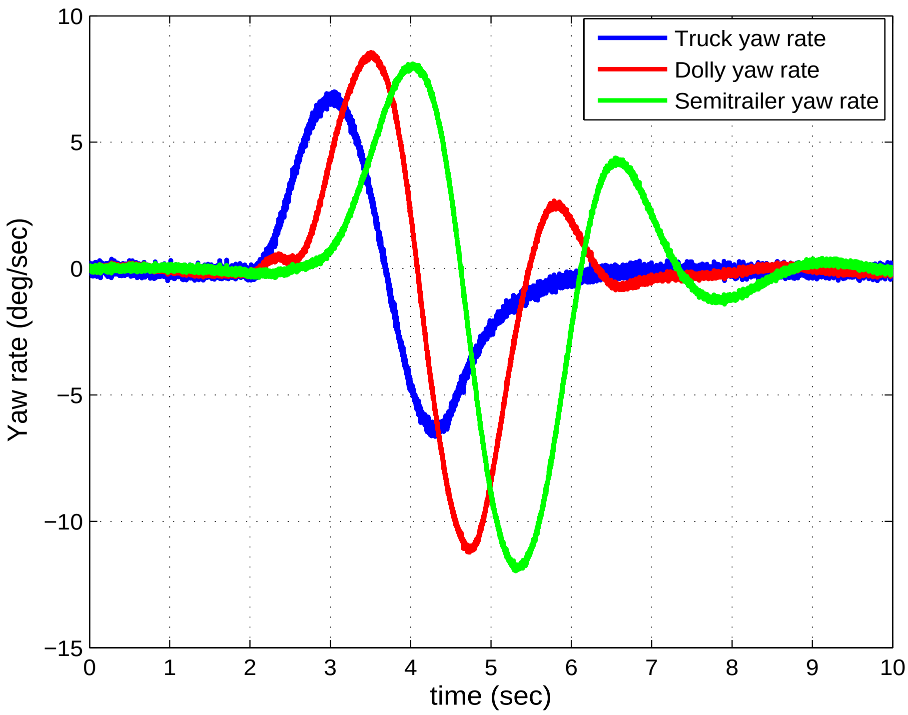

Figure 4.1: Yaw rate responses of the truck (blue), dolly (red) and semitrailer (green) for passive case.

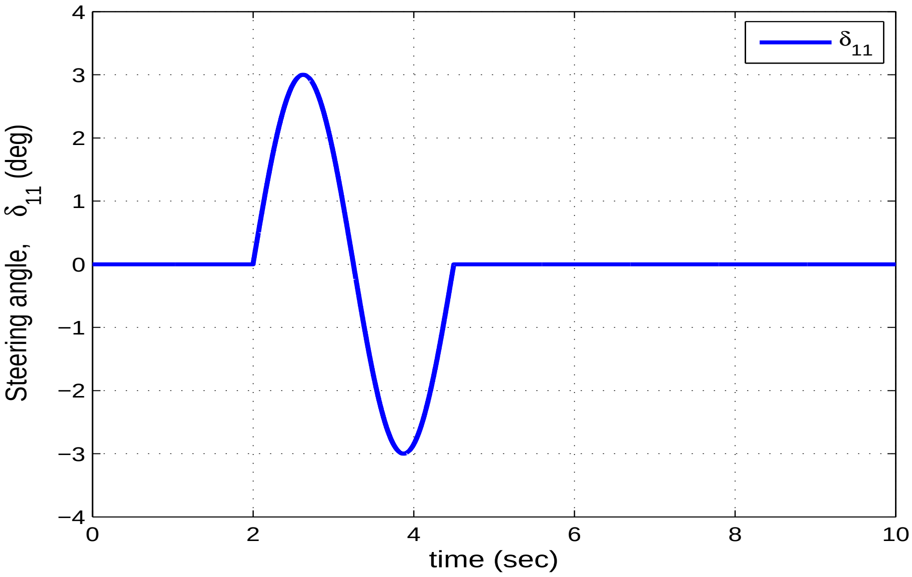

Figure 4.2: Steering angle of the front axle of the truck, refer to Figure 4.1

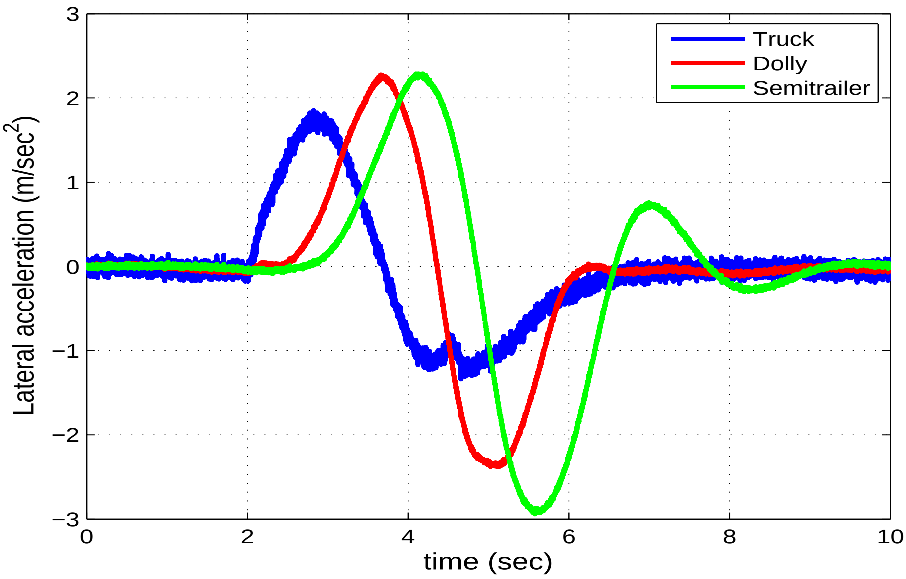

.

Figure 4.3: Lateral acceleration of the truck (blue), dolly (red) and semitrailer (green) for passive case.

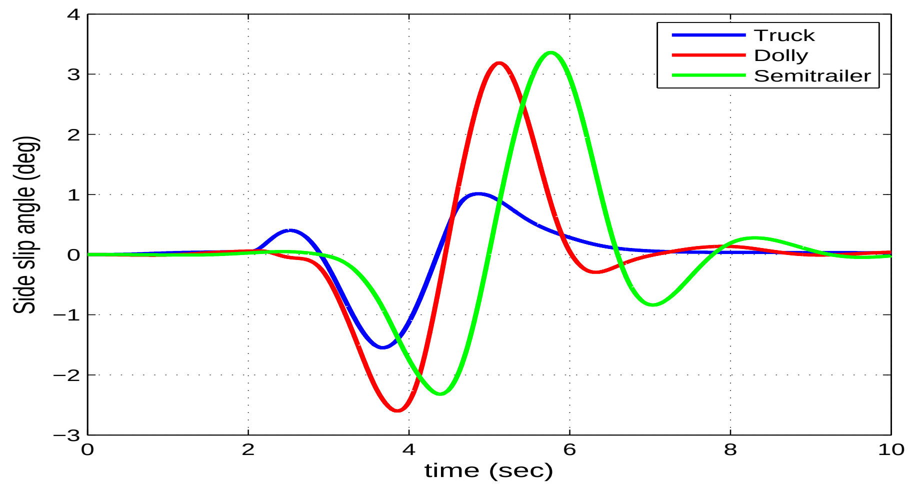

Figure 4.4: Side slip angle of the truck (blue), dolly (red) and semitrailer (green) for passive case.

In Figure 4.6 the yaw rate responses for Controller A are illustrated when the steering profile in Figure 4.2 is implemented. As shown, the yaw rate of the dolly and semitrailer satisfactory track their corresponding reference signals by reducing the RWA, compared to the passive case as reported in Table 4.3. The lateral accelerations and side slip angles RWA are also reduced, as shown in Figure 4.7 and 4.8 compared to the passive case. Finally, the off-tracking is considerably reduced compared to the passive case, as depicted in Figure 4.10.

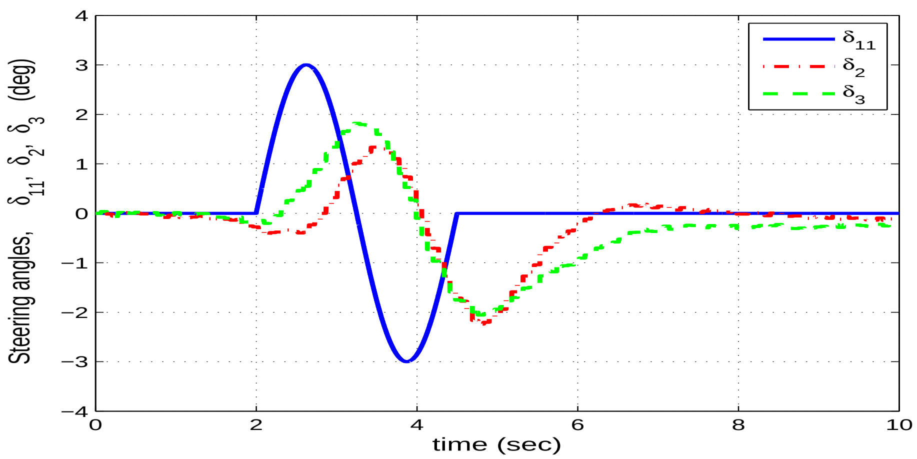

Figure 4.5: Steering angles of the truck (blue), dolly (red) and semitrailer (green) for Controller A.

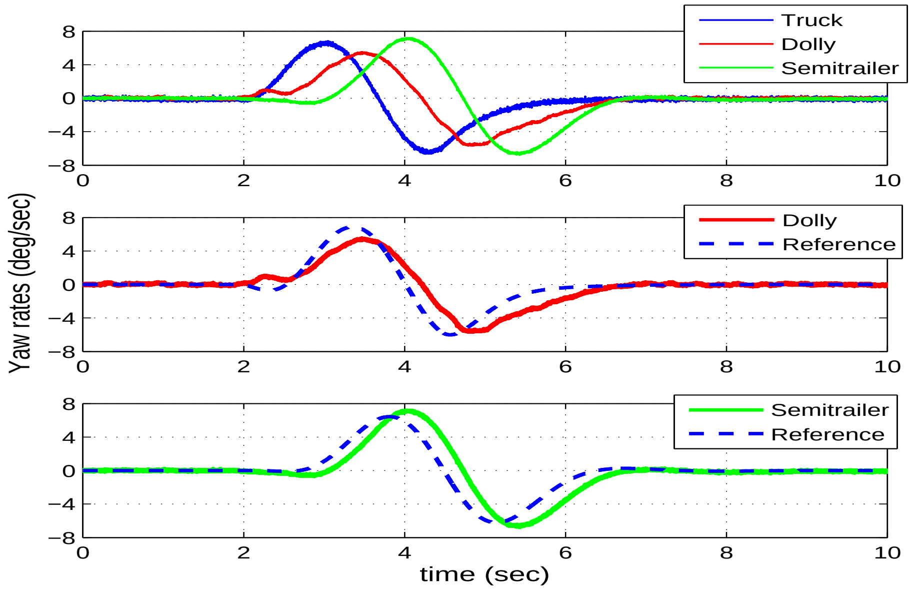

Figure 4.6: In the upper plot are the yaw rates of the truck (blue), dolly (red) and semitrailer (green) for Controller A. In the middle plot, the yaw rates of the dolly (red) is compared against its reference (dashed line). In the lower plot, the yaw rate of the semitrailer (green) is compared against its reference (dashed line).

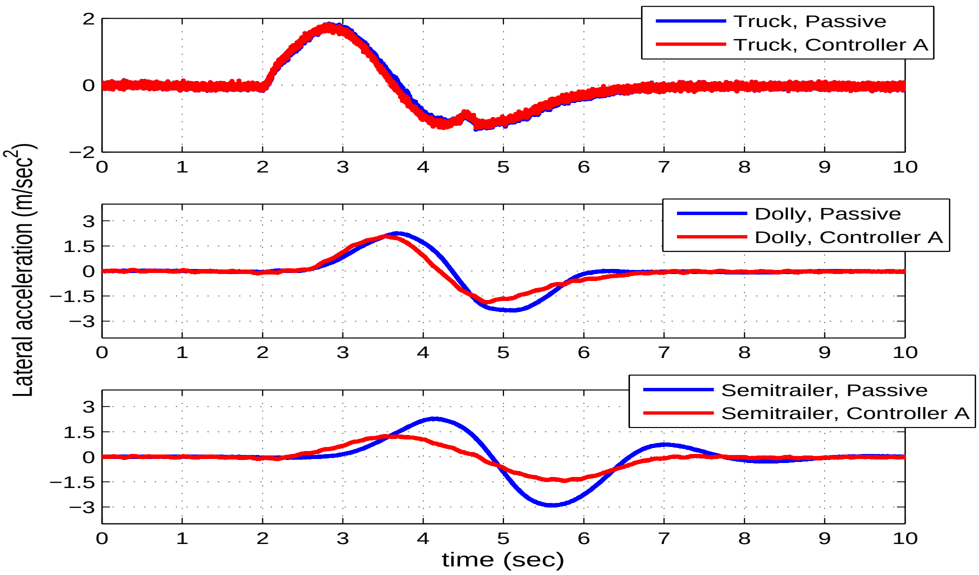

Figure 4.7: Lateral acceleration of each unit for Controller A is compared to the corresponding lateral acceleration in passive case.

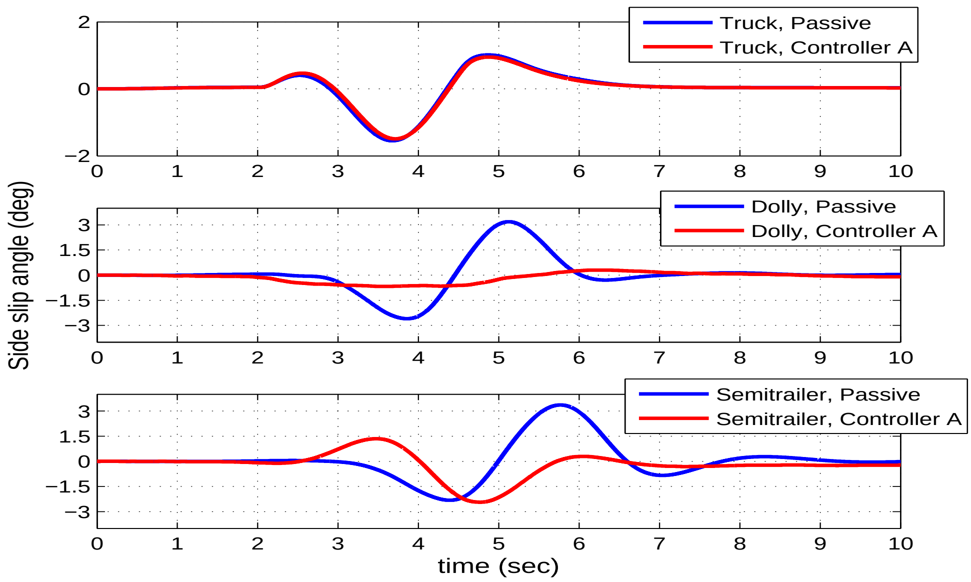

Figure 4.8: Side slip angle of of each unit for Controller A is compared to the corresponding Side slip angle in passive case.

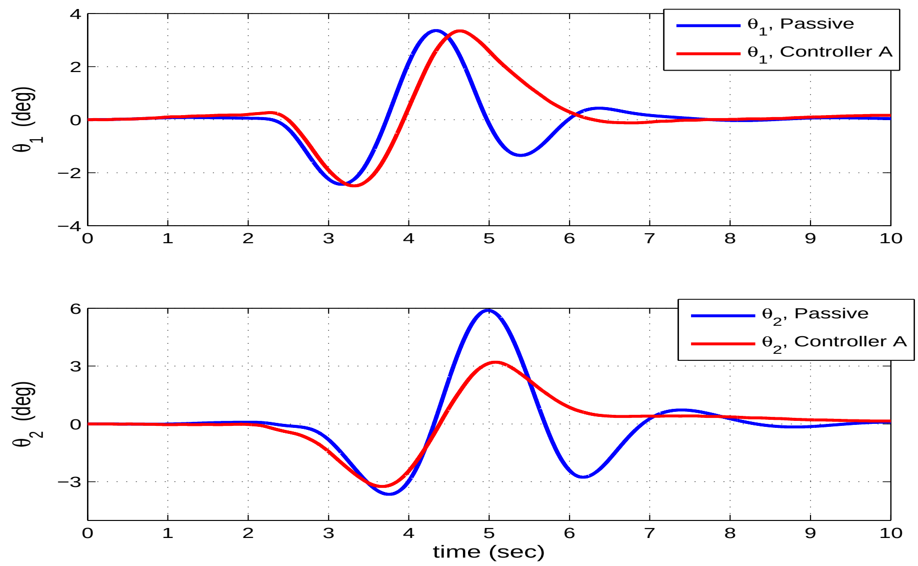

Figure 4.9: First articulation angle θ_1 (upper plot) and second articulation angle θ_1 (lower plot) for Controller A versus their respective signals for passive case .

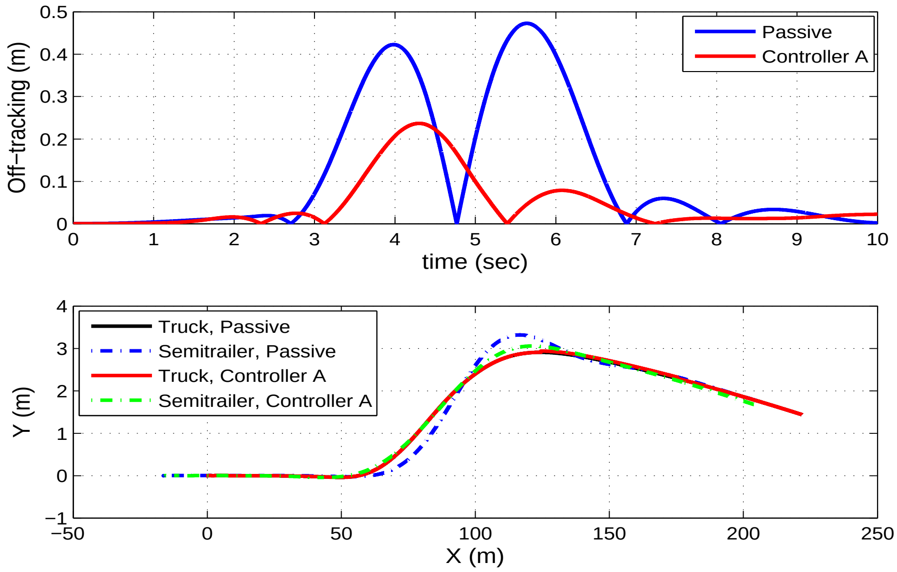

Figure 4.10: upper plot is the Off-tracking of the vehicle for Controller A versus passive case Lower plot is the truck and semitrailer paths for both Controller A and passive case.

By analyzing the articulation angles θ_1 and θ_2 in Figure 4.9 , we observe that, despite the good tracking performance, the Controller A could lead to an unacceptable misalignment of the three units at the end of the single lane change, when δ_{11} is zero and the articulation angles should converge to zero. The non zero steering angles, δ_2 and δ_3, and articulation angles, θ_1 and θ_2, after 6 s, in Figures 4.5 and 4.9, respectively, correspond to the vehicle configuration depicted in Figure 4.11 where the three units are not aligned. The misalignment of the three units occurs when the vehicle terminates the single lane change with non-zero articulation and steering angles. In particular, at the end of the maneuver the yaw rate references are zero and, for a given set of tuning parameters, setting the steering angles to zero would increase the yaw rates tracking errors.

A similar situation occurs at the beginning of the simulation. In Figure 4.5, we observe an initial drift in the steering angle of the dolly and semitrailer, corresponding to the drifting articulation angles in Figure 4.9. This controller behavior is artificially induced by slightly steering the rearmost axle of the truck[1]. In order to keep the yaw rates of the dolly and semitrailer constantly at zero, the controller compensates for the steering at the truck,

[1]Steerability in the rearmost axle of the truck has been considered in the vehicle model for other applications.

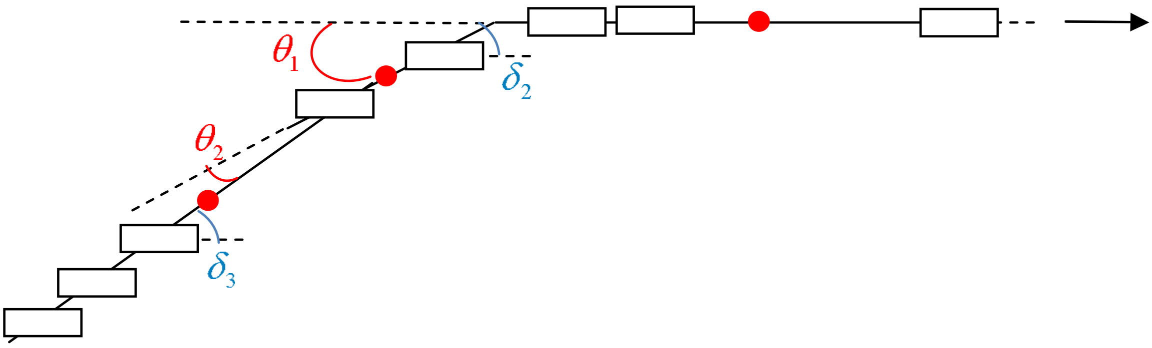

Figure 4.11: Vehicle configuration sketch describing the alignment of the three units at the end of a single lane change maneuver.

by slightly decreasing δ_2 and δ_3.

Such undesired behavior of Controller A can be alleviated by either increasing the weights on the steering angles (i.e., the diagonal elements in the matrix S, shown in 4.3), introducing an integral action in the controller or tracking the articulation angles as well.

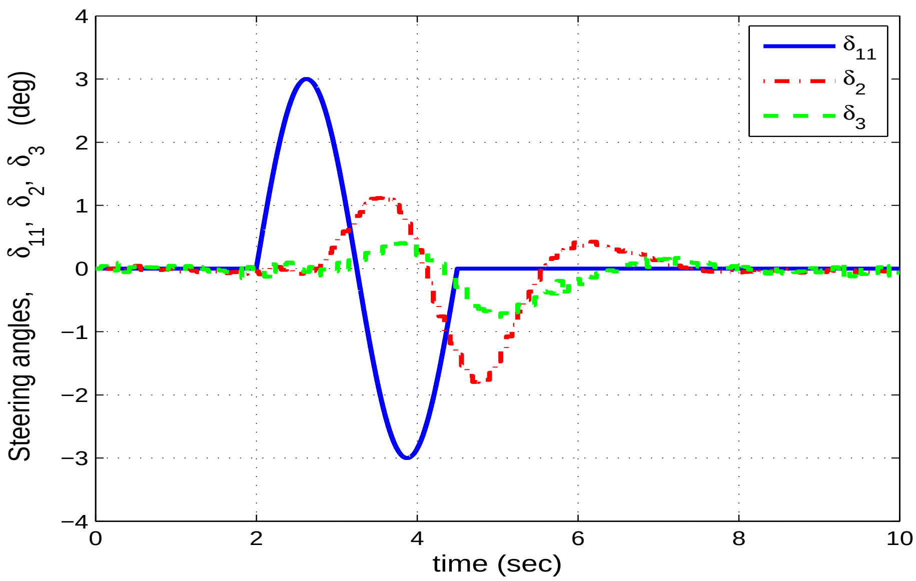

Figure 4.12: Steering angles of the truck (blue), dolly (red) and semitrailer (green) for Controller B.

The problem sketched in Figure 4.11 is solved in Controller B, by tracking articulation angles references as well. In particular, the tracking of the articulation angles forces the controller to align the three units after the single lane change, when the articulation angles references are zero. The reference signals for articulation angles are computed as 4.2. The yaw rates and the articulation angles in Figures 4.13 and 4.16, respectively, show that reduction of yaw rate RWA is achieved by implementing Controller B while correctly aligning the three units at the end of the single lane change. This is also confirmed by looking at Figure 4.12 where the initial drifts and final offsets on the steering angles of the dolly and the semitrailer are no longer observed.

Moreover, we observe that the lateral accelerations and side slip angles as illustrated in Figures 4.14 and 4.15, respectively, are improved compared to the passive case. The off-tracking is also reduced to almost one half of its value in passive case, as shown in Figure 4.17.

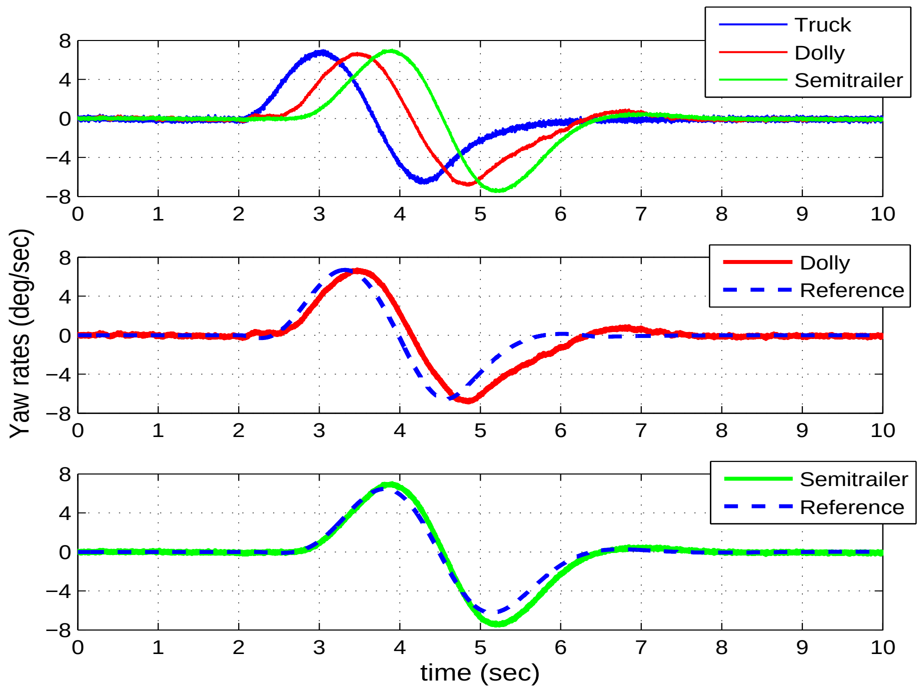

Figure 4.13: In the upper plot are the yaw rates of the truck (blue), dolly (red) and semitrailer (green) for Controller B. In the middle plot, the yaw rates of the dolly (red) is compared against its reference (dashed line). In the lower plot, the yaw rate of the semitrailer (green) is compared against its reference (dashed line).

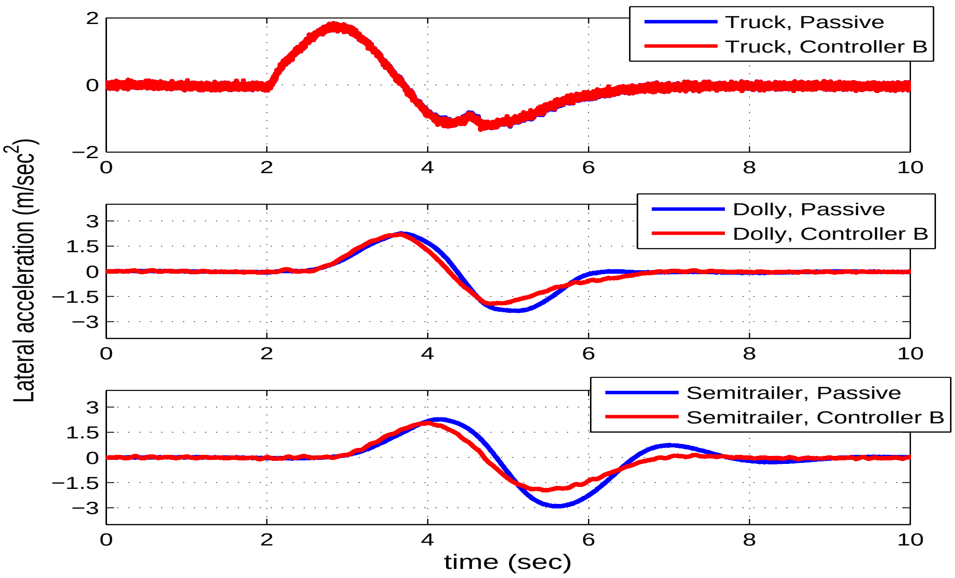

Figure 4.14: Lateral acceleration of each unit for Controller B is compared to the corresponding lateral acceleration in passive case.

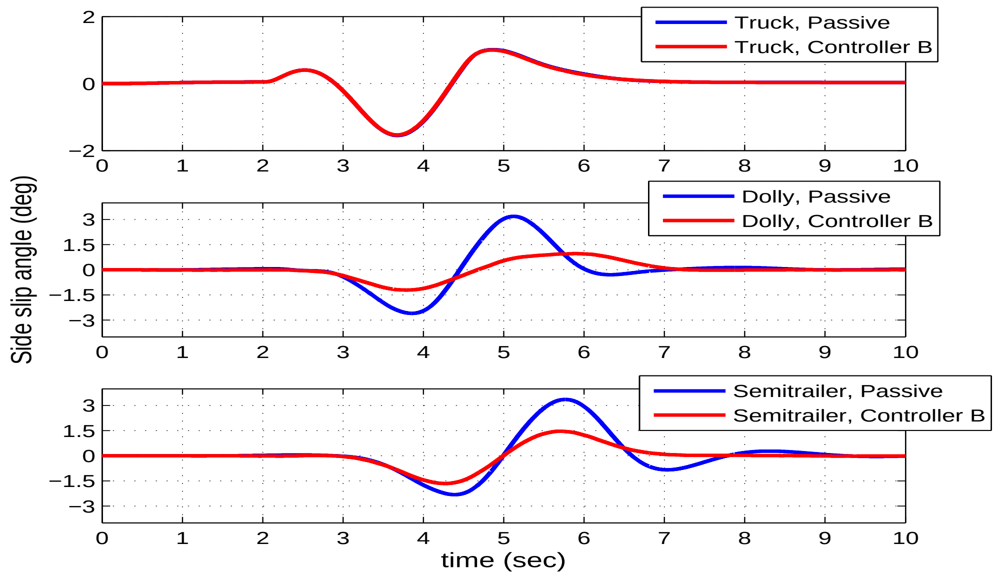

Figure 4.15: Side slip angle of of each unit for Controller B is compared to the corresponding Side slip angle in passive case.

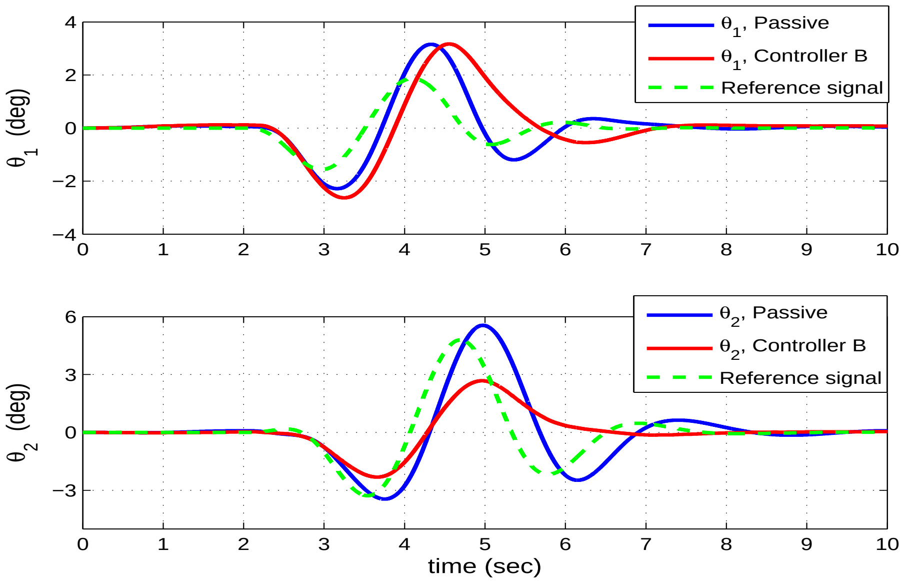

Figure 4.16: First articulation angle θ_1 (upper plot) and second articulation angle θ_1 (lower plot) for Controller B versus their respective signals for passive case .

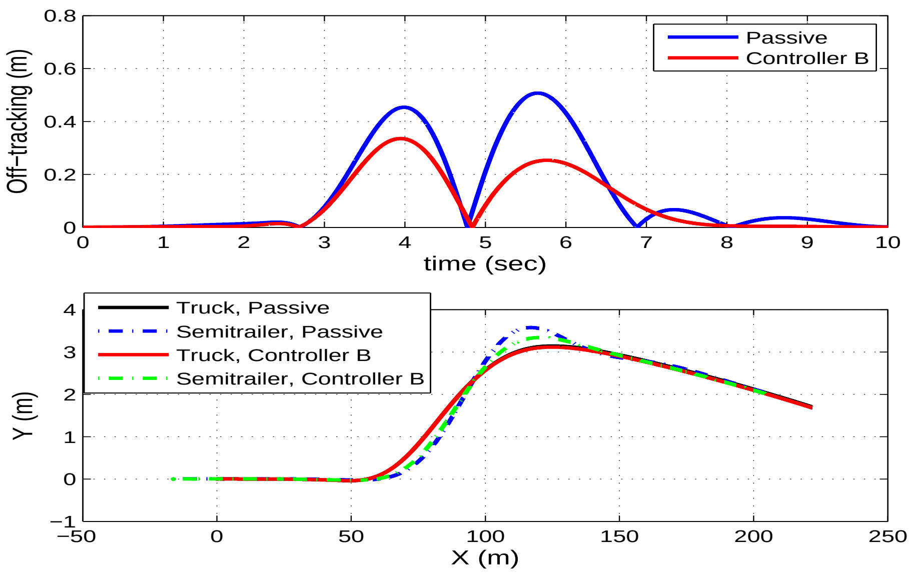

Figure 4.17: upper plot is the Off-tracking of the vehicle for Controller B versus passive case. Lower plot is the truck and semitrailer paths for both Controller B and passive case.

In Table 4.3 we summarize the results obtained by implementing two controllers. By analyzing the results reported in Table 4.3, we conclude that the performance of Controller A is slightly better than Controller B in terms of reducing the RWA for the yaw rates, lateral accelerations and side slip angles, as well as the off-tracking. However, implementing Controller B, the proper alignment of the three units at the end of the single lane change maneuver can be promised.

	Passive Case	Controller A	Controller B
$\mathrm{RWA}_{\dot{\psi},2}$	1.65	0.84	1.03
$\mathrm{RWA}_{\dot{\psi},3}$	1.7	1.03	1.1
$\mathrm{RWA}_{a_y,2}$	1.78	1.34	1.45
$\mathrm{RWA}_{a_y,3}$	2.19	1.14	1.47
$\mathrm{RWA}_{\beta,2}$	3.15	0.45	0.97
$\mathrm{RWA}_{\beta,3}$	3.32	1.63	1.46
Max(OT) $[m]$	0.64	0.23	0.32

Table 4.3: Comparison of the results obtained from Passive case with the results for Controller A and Controller B. In $RWA_{\star,\bullet}$, $\star$ denotes the motion variable the RWA is referred to and $\bullet$ denotes the unit, i.e., dolly or semitrailer. The symbol OT denotes the off-tracking.

4.3.2 Experimental Results

In this section we present and discuss the experimental results obtained from testing the designed MPC controller on an experimental vehicle[2]. Controller B, presented in Section 4.3, was used in the experimental testing. A single lane change maneuver is considered at 80 kph on a dry road.

We remark that the experimental results presented in this section, are the preliminary results obtained during limited number of testing.

In Figure 4.18 the experimental results are shown. We observe that the reduction of the RWA for the yaw rate of the dolly and semitrailer has been achieved. Moreover, considering Figures 4.19 and 4.20, the good reference tracking for the yaw rate of the dolly and semitrailer, respectively, can be verified.

[2]Experimental testing has been performed at Mira test center in England.

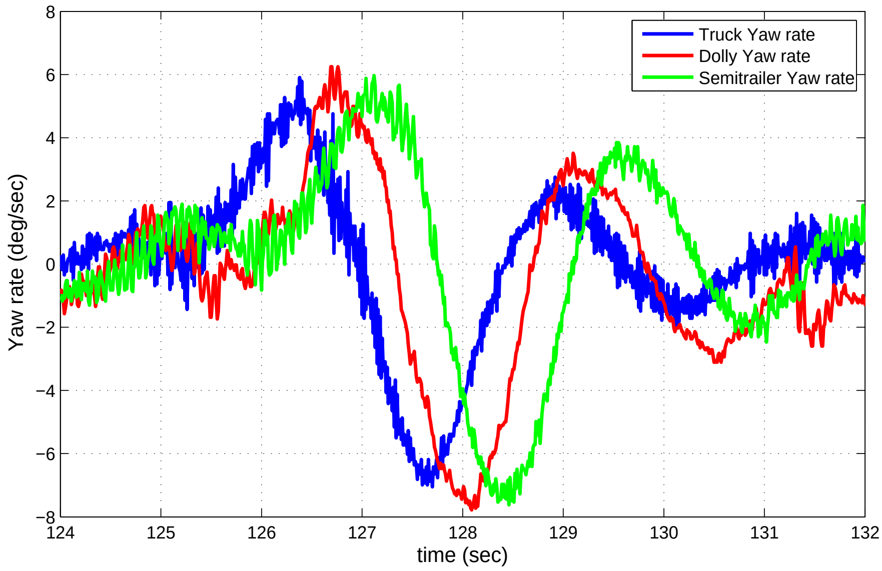

Figure 4.18: Yaw rate responses for each unit of the combination.

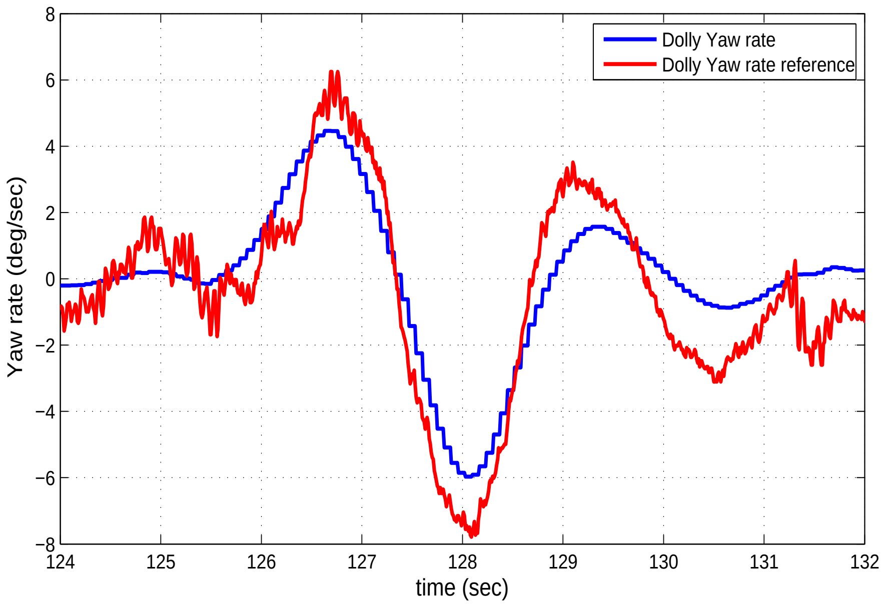

Figure 4.19: Yaw rate of the dolly versus its reference signal.

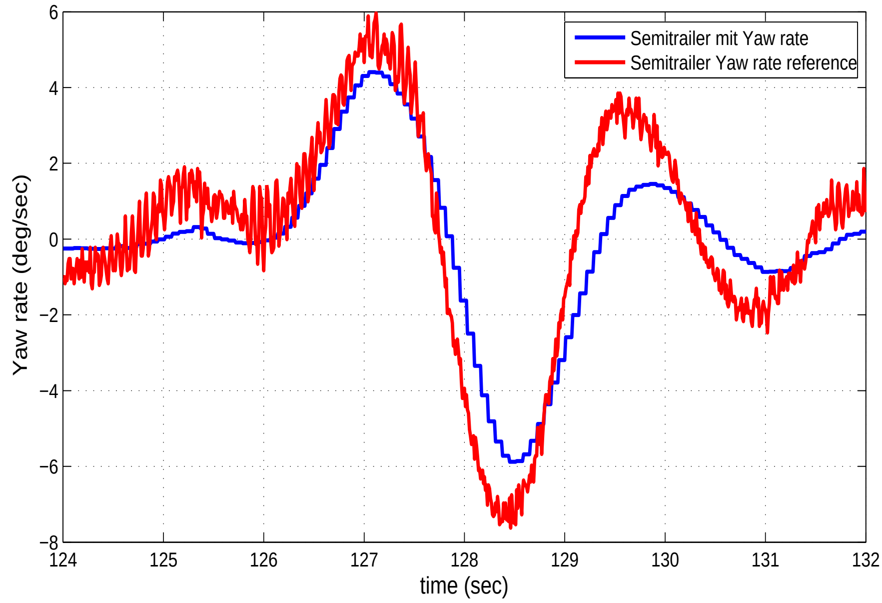

Figure 4.20: Yaw rate of the semitrailer versus its reference signal.

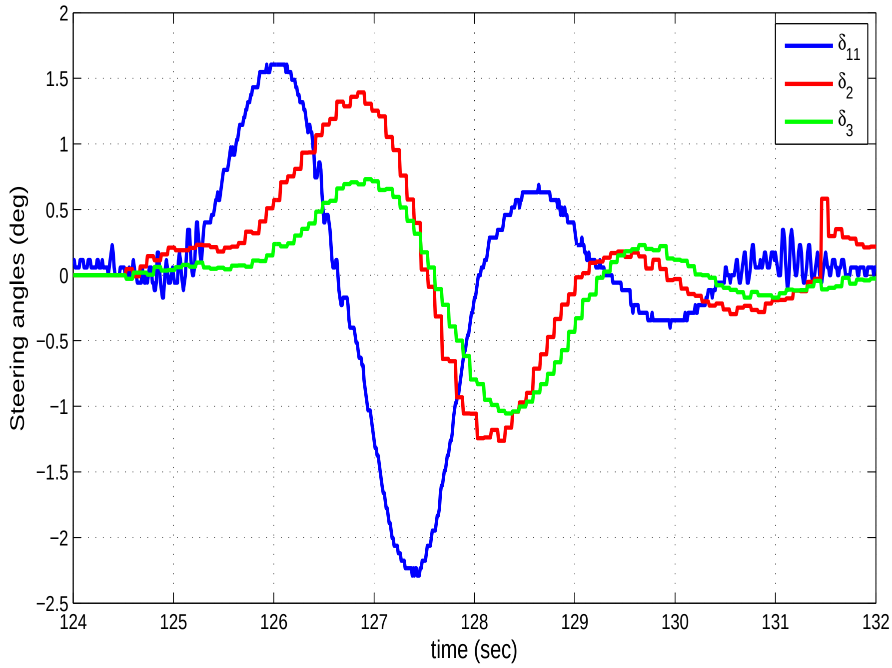

Figure 4.21: Steering commands for the dolly and the semitrailer.

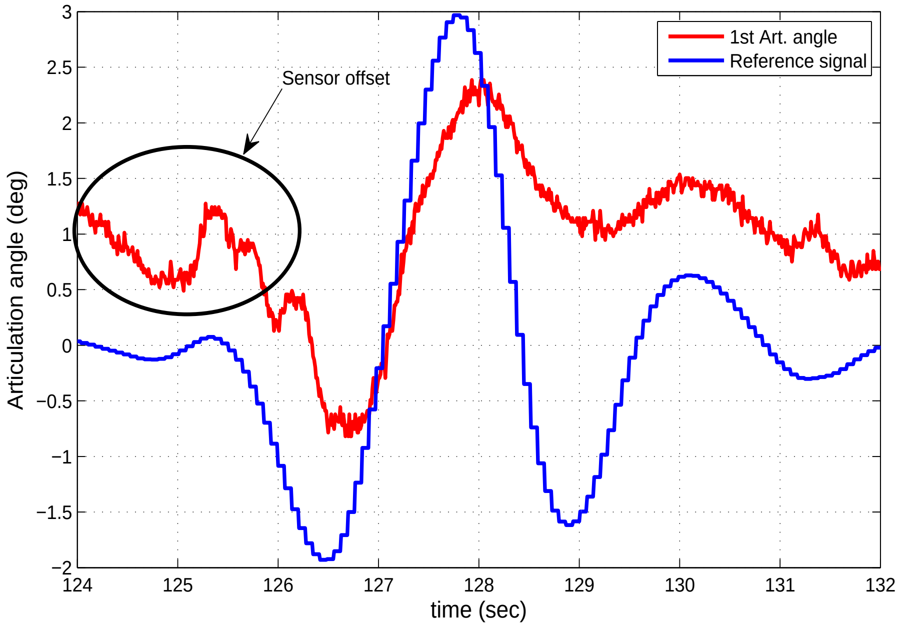

Figure 4.22: First articulation angle versus its reference signal.

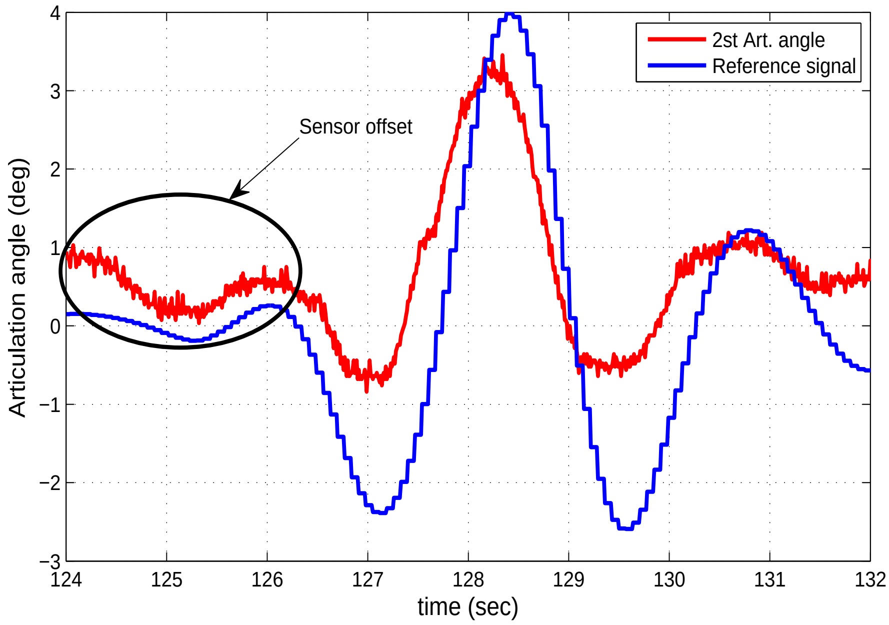

Figure 4.23: Second articulation angle versus its reference signal.

By analyzing the yaw rates in Figure 4.18, we conclude that the controller is considerably robust in terms of dealing with sensor noises. This can be also confirmed by smooth steering commands at the dolly and the semitrailer, reported in Figure 4.21. It is worth to mention that there is no filter to remove the noises from feedback states and the controller design alone is enough to guarantee a good performance when facing noisy signals.

Finally the articulation angles are shown in Figures 4.22 and 4.23. As highlighted in these figures, we observe that there are sensors offset of almost 1 degree in the articulation angles. Such offsets in the articulation angles could affect the controller performance in terms of nonzero steering commands for the dolly and semitrailer at straight driving. For the experimental testing, this problem was primarily solved by decreasing the weights on the articulation angles in the object function (i.e., two last elements of the matrix S, reported in 4.3). So that the offset would affect the steering commands when the yaw rates tracking errors converge to zero.

By analyzing the articulation angles in Figures 4.22 and 4.23, we observe that, despite of the sensors offset at articulation angles, the correct alignment of the three units at the end of the single lane change maneuver has been achieved, i.e., the sensor offsets before and after the maneuver are the same. We point out that the controller was turned off immediately when the vehicle terminated the lane change maneuver and we were not able to investigate the effect of sensors offset on the controller performance in straight driving. It is also worth mentioning that by penalizing the articulation angles in the object function, we were mainly aiming for correct alignment of the three units at steady state and good reference tracking for the articulation angles was not the purpose.

We remark that there would be improvements for the controller in terms of dealing with sensors offset, particularly, in straight driving such as design and implementation of a state observer to estimate offset free articulation angles.

4.4 Real-Time Implementation of the Model Predictive Vehicle Dynamics Control

In this section we outline the steps for implementing the designed MPC controller on a vehicle for experimental testing. The real-time testing has been carried out by using Real Time Workshop, RTW, present in Matlab R2007b and XPC target environment. All the real time applications are developed in Simulink similar to the offline simulations. The MPC controller developed for the real-time application is the user defined C-coded S-function. The optimization problem is solved by using the LSSOL package which solves the quadratic programming problems. LSSOL consists of a series of optimization routines, and for more information consult [20].

4.4.1 Hardware

The XPC target system is a real-time computing system, with different I/O capabilities, used for rapid prototyping in automotive applications. The real-time application is developed in Simulink through the built-in Simulink blocks and additional Real Time Implementation (RTI) libraries for manag-

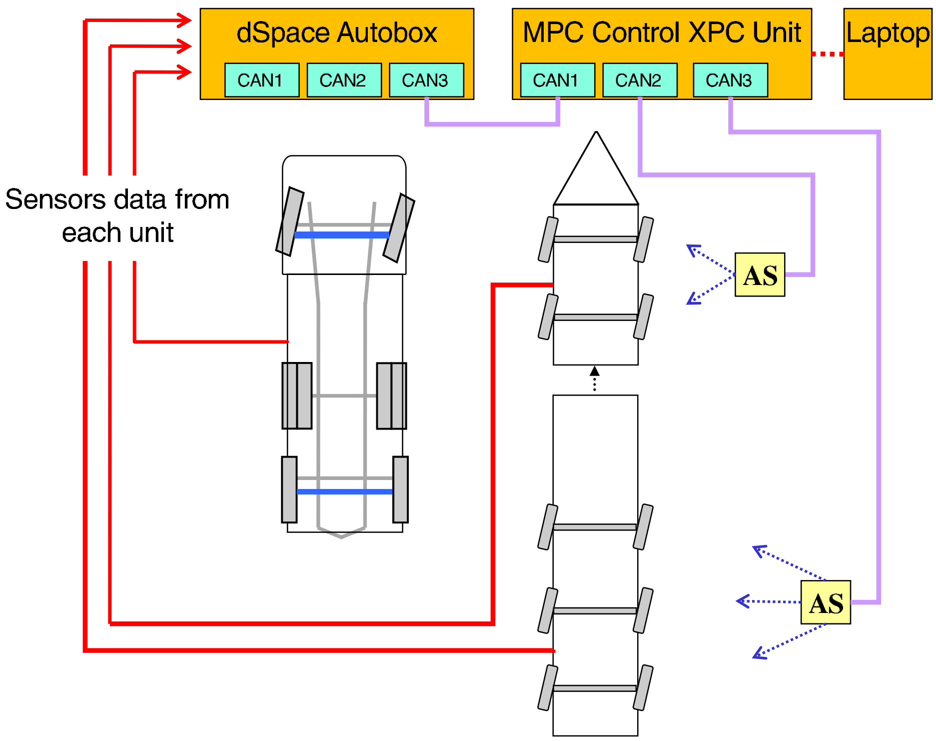

Figure 4.24: First articulation angle θ_1 (upper plot) and second articulation angle θ_1 (lower plot) for real-time implementation in one XPC computer.

ing the processing and I/O hardware. After the building process, performed with Mathworks Real-Time Workshop (RTW), the executable file is automatically downloaded into the XPC target computer and executed in real-time [4]. The target computer in this application is a Pentium 4 with 2:4GHz and 512mB of available RAM.

4.4.2 The XPC Target Experimental Setup

In Figure 4.24 the experimental setup, based on a XPC target system, is shown. We observe a dSpace Autobox which is mounted on the truck and the XPC target control unit. A dSpace system, similar to XPC target, is a real-time computing system which is devised in the truck for other purposes. However, all the sensor data from the three units are sent to the dSpace system.

The XPC control unit and dSpace system communicate through the available CAN bus. All the required signals for the XPC control unit including the state vector (2.15) and steering angles, δ_{11}, δ_2 and δ_3, are provided by the dSpace and via CAN communication. In particular, every sample time the XPC control unit send the current steering commands, δ_2 and δ_3, to the steering actuators at the dolly and the semitrailer.

The designed MPC algorithm is executed in real-time at a frequency of 100 Hz. This frequency has been selected as a trade-off between performance and computational complexity.

Chapter 5

Conclusion

This thesis work proposed a vehicle dynamic control problem in long combinations of heavy vehicles. The MPC approach was considered to improve the lateral instability in such configurations. Using MPC was motivated by its capability of dealing with the constraints at the steering actuators while providing optimal control action. Mainly, we focused on reducing the yaw rate RWA at two last units with respect to the truck, in a truck-dolly-semitrailer combination.

We presented two MPC controllers for proposed vehicle dynamic problem. In first controller, referred to Controller A, we introduced yaw rate tracking problem at the dolly and the semitrailer. However, this controller could lead to an unacceptable misalignment of the three units. To guarantee the correct alignment of the three units at the end of a single lane change maneuver, we introduced Controller B tracking both the yaw rates and articulation angles.

5.1 Summary of Results

Based on the vehicle model linearization introduced in 2.2.1, the yaw rate reference models for the dolly and semitrailer were generated such that the reductions of yaw rates RWA at the dolly and semitrailer are achieved, $RWA < 1$, while the natural phase lags of the dolly and semitrailer were promised. By analyzing the results of Controller A, shown in 4.3.1, we conclude that, despite the good tracking performance of Controller A, the correct alignment of the vehicle units was not guaranteed at the end of the single lane change maneuver; nonzero articulation and steering angles after 6 s in Figures 4.9 and 4.5, respectively. This problem as sketched in 4.11 was solved by tracking both the yaw rates and articulation angles in Controller B. The reference signals for articulation angles were generated by integrating and subtracting the yaw rate reference signals as in (4.2). Although the simulation results of Controller B were slightly worse than Controller A in terms of reducing the yaw rate RWA and off-tracking, as reported in Table 4.3, the performance of Controller B was more consistent. That is, the correct alignment of the three units at the end of a single lane change maneuver can be promised.

Next, the C-coded Controller B was implemented on a vehicle for real testing of the controller. An XPC target environment was used as the real-time computing system in experimental testing. Finally in Section 4.3.2, the results obtained from the real testing of the controller on a truck were presented. The successful development and implementation of the controller for a real application was approved through the given results. Nevertheless, we remark that there would be improvements on the controller in terms of dealing with the sensors offset in steady state; straight driving.

Note that in this thesis we studied the basic possibilities of using Model Predictive Control approach to yaw dynamics stabilization in long heavy vehicles combinations and there are open areas for future works.

5.2 Future Works

To guarantee the reduction of yaw rate RWA at the dolly and semitrailer below 1, additional constraints could be included bounding the deviation of the dolly and semitrailer yaw rate from the reference signals.

Improving the dolly and semitrailer yaw rates might cause other stability issues for the vehicle combination, i.e., rollover due to excessive lateral accelerations. To solve this problem, an additional set of constraints bounding the lateral acceleration in each unit of the combination could be addressed.

The steerability of the rearmost axle of the truck could be considered as another control input. Moreover, the advantage of using individual steering at each single axle of towed units could be investigated. This would require removing the simplifying assumption of lumped axles at the dolly and semitrailer presented in Remark 1.

Good tracking performance of the controller was concluded by minimal design and tuning efforts. However, there would be improvements on the controller by spending more efforts and time on tuning parameters.

Another interesting proposal for future is simultaneously reducing the yaw rate and lateral acceleration RWA and off-tracking. That is, along with bounding yaw rates and lateral accelerations, an additional constraint to limit the off-tracking might be included in the MPC formulation as well.

The reference signals in MPC algorithm are of crucial importance. Instead of tuning the yaw rates transfer functions to the truck steering, a more systematic way could be utilized to generate the reference signals.

Future work will be also dedicated to investigate the advantage of combining steering and braking interventions. This could be further extended to include the dynamics of the braking system in the vehicle model.

Future steps of experimental testing will aim at investigating the robustness of the proposed controller with respect to vehicle uncertainty, variation of the road friction and sensors offset. Design and implementation of an observer to estimate the sensors offset could be a solution to deal with the sensors offset in real applications, particularly, in straight driving.

The presented work was a core study to investigate the possibilities of using MPC approach to develop a lateral stability controller for longer heavy vehicles combinations. The vehicle configuration could be extended up to 5 or 6 units. Such longer combinations would lead to a much more complicated vehicle dynamic control problem for which MPC algorithm could be a proper solution.

Bibliography

[1] Government of south Australia, Heavy vehicle road transport, *Office of the Economic Development Board*, August 2008.

[2] K. Ramberg, Confederation of Swedish Enterprise. *Fewer Trucks Improve the Environment.*, October 2004.

[3] S. Kharrazi.*On Lateral Stability of Heavy Vehicle Combinations.* Licentiate thesis, Chalmers University of Technology, Gothenburg, 2008.

[4] P. Falcone.*Nonlinear Model Predictive Control for Autonomous Vehicles.* PhD thesis, University of Sannio, Benevento, 2007.

[5] B. Schofield, M. Lidberg.*Derivation of Linear Single-track Truck-Dolly-Semitrailer Model with Steerable Axles.* Technical Report, Feburary 2010.

[6] ISO, *Road vehicles heavy commercial vehicle combinations and articulatedbuses lateral stability test methods*, Swedish Standard Institute,Std. SS-ISO 14 791, 2002.

[7] R. Findeisen, F. Allgöwer, *An Introduction to Nonlinear Model Predictive Control* ,Institute for Systems Theory in Engineering,University of Stuttgart, Germany.

[8] E.F Camancho and C. Bordons. *Model Predictive Control.*, Springer, 2006.

[9] J.M. Maciejowski. *Predictive Control with Constraints.*, Prentice Hall, 2000.

[10] R. Shridhar and D. J. Cooper.*A Tuning Strategy for Unconstrained SISO Model Predictive Control.*, Ind. Eng. Chem. Res. 1997, 36, 729-746.

[11] P. Gill, S.J. Hammarling, W. Murray, M. A. Saunders, and M. H. Wright. *Users guide for lssol (version 1.0): A fortran package for constrained linear least-squares and convex quadratic programming.*, Technical report, 1986.

[12] K.J. Åström, B. Wittenmark, *Computer Controlled Systems.*, Prentice Hall, 1997.

[13] P. Nordengen, H. Prem, L. Mai, *An initiative to introduce a Performance-Based Standards(PBS) approach for heavy vehicle design and operations in South Africa.*, 2008.

[14] H. B. Pacejka, *Tire and Vehivle Dynamics*, Elsevier Butterworth-Heinemann, Oxford, 2004.

[15] B. D. Agusto, R. J. Loureiro, *Motion Cueing in the Chalmers Driving Simulator: A Model Predictive Control Approach.*, Master thesis,Chalmers University of Technology, Gothenburg, 2009.

[16] S. Kharrazi and R. Thomson, *Study of heavy truck accidents with focus on maneuvers causing loss of control.*, International Journal of Vehicle Safety, vol. 3, no. 1, pp. 3244, 2008.

[17] P. Fancher, C. Winkler, R. Ervin, and H. Zhang, *Using braking to control the lateral motions of full trailers.*, Vehicle System Dynamics, vol. 29, pp. 46278, 1998.

[18] L. Palkovics and M. El-Gindy, *Design of an active unilateral brake control system for five-axle tractor-semitrailer based on sensitivity analysis.*, Vehicle System Dynamics, vol. 24, pp. 725758, 1995.

[19] C. Cheng and C. D., *Improving roll stability of articulated heavy vehicles using active semi-trailer steering.*, Vehicle System Dynamics, vol. 46, no. 1, pp. 373388, 2008.

[20] P. Gill, S.J. Hammarling, W. Murray, M. A. Saunders, and M. H. Wright, *Users guide for lssol (version 1.0): A fortran package for constrained linear least-squares and convex quadratic programming.*, Technical report, 1986.

[21] http://www.pacontrol.com/MPC.html, 2009.

Appendix A

Parameter Varying Matrices for Linear Models

In this section we present the linear parameter varying matrices for the linear models introduced in section 2.2.

A.1 Linear Model derived by Newtonian Method

The state space matrices defined in the linear model 2.11 are as below:

$$M_s(p) = \begin{bmatrix} d_{1r}m_1p & -I_{z_1} & 0 & 0 & 0 & 0 \\ 0 & 0 & 0 & 0 & d_{3f}m_3p & -I_{z_3} \\ m_1p & 0 & m_2p & 0 & m_3p & 0 \\ d_{2f}m_1p & 0 & 0 & I_{z_2} & d_{2r}m_3p & 0 \\ 1 & \frac{d_{1r}}{p} & -1 & -\frac{d_{2f}}{p} & 0 & 0 \\ 0 & 0 & 1 & \frac{d_{2r}}{p} & -1 & -\frac{d_{3f}}{p} \end{bmatrix}, \tag{A.1a}$$

$$A_s(p) = \begin{bmatrix} F_{\beta_1}d_{1r} - M_{\beta_1} & 0 & F_{\beta_1} & F_{\beta_1}d_{2f} & 0 & 0 \\ F_{\dot{\psi}_1}d_{1r} - M_{\dot{\psi}_1} - d_{1r}m_1p & 0 & F_{\dot{\psi}_1} - m_1p & F_{\dot{\psi}_1}d_{2f} - d_{2f}m_1p & 1 & 0 \\ 0 & 0 & F_{\beta_2} & M_{\beta_2} & 0 & 0 \\ 0 & 0 & F_{\dot{\psi}_2} - m_2p & M_{\dot{\psi}_2} & -1 & 1 \\ 0 & F_{\beta_3}d_{3f} - M_{\beta_3} & F_{\beta_3} & F_{\beta_3}d_{2r} & 0 & 0 \\ 0 & F_{\dot{\psi}_3}d_{3f} - M_{\dot{\psi}_3} - d_{3f}m_3p & F_{\dot{\psi}_3} - m_3p & F_{\dot{\psi}_3}d_{2r} - d_{2r}m_3p & 0 & -1 \end{bmatrix}^T, \tag{A.1b}$$

$$B_s(p) = \begin{bmatrix} 0 & 0 & -F_{\beta_2} & -M_{\beta_2} & 0 & 0 \\ 0 & M_{\beta_3} - F_{\beta_3} d_{3f} & -F_{\beta_3} & -F_{\beta_3} d_{2r} & 0 & 0 \end{bmatrix}^T, \tag{A.1c}$$

$$E_s(p) = \begin{bmatrix} C_{11}(d_{1r} - l_{11}) & 0 & C_{11} & C_{11} d_{2f} & 0 & 0 \end{bmatrix}^T. \tag{A.1d}$$

A.2 Linear Model derived by Lagrange Method

The state space matrices defined in the linear model 2.22 are as below:

$$M_b(p) = \begin{bmatrix} M_{b_{11}} & M_{b_{12}} & M_{b_{13}} & M_{b_{14}} & M_{b_{15}} & M_{b_{16}} \\ M_{b_{21}} & M_{b_{22}} & M_{b_{23}} & M_{b_{24}} & M_{b_{25}} & M_{b_{26}} \\ M_{b_{31}} & M_{b_{32}} & M_{b_{33}} & M_{b_{34}} & M_{b_{35}} & M_{b_{36}} \\ M_{b_{41}} & M_{b_{42}} & M_{b_{43}} & M_{b_{44}} & M_{b_{45}} & M_{b_{46}} \\ M_{b_{51}} & M_{b_{52}} & M_{b_{53}} & M_{b_{54}} & M_{b_{55}} & M_{b_{56}} \\ M_{b_{61}} & M_{b_{62}} & M_{b_{63}} & M_{b_{64}} & M_{b_{65}} & M_{b_{66}} \end{bmatrix}, \tag{A.2}$$

$$A_b(p) = \begin{bmatrix} A_{b_{11}} & A_{b_{12}} & A_{b_{13}} & A_{b_{14}} & A_{b_{15}} & A_{b_{16}} \\ A_{b_{21}} & A_{b_{22}} & A_{b_{23}} & A_{b_{24}} & A_{b_{25}} & A_{b_{26}} \\ A_{b_{31}} & A_{b_{32}} & A_{b_{33}} & A_{b_{34}} & A_{b_{35}} & A_{b_{36}} \\ A_{b_{41}} & A_{b_{42}} & A_{b_{43}} & A_{b_{44}} & A_{b_{45}} & A_{b_{46}} \\ A_{b_{51}} & A_{b_{52}} & A_{b_{53}} & A_{b_{54}} & A_{b_{55}} & A_{b_{56}} \\ A_{b_{61}} & A_{b_{62}} & A_{b_{63}} & A_{b_{64}} & A_{b_{65}} & A_{b_{66}} \end{bmatrix}, \tag{A.3}$$

$$B_b(p) = \begin{bmatrix} d_{2r} & C_3 \\ d_{2r}(-d_{1r} - d_{2f} - l_{22}) & C_3(-d_{1r} - l_2 - d_{3f} - l_{32}) \\ -d_{2r}(d_{2f} + l_{22}) & -C_3(d_{3f} + l_2 + l_{32}) \\ 0 & -C_3(d_{3f} + l_{32} \\ 0 & 0 \\ 0 & 0 \end{bmatrix}$$

$$E_b(p) = \begin{bmatrix} C_{11} & C_{11} l_{11} & 0 & 0 & 0 & 0 \end{bmatrix}^T \tag{A.4}$$

where,

$$
\begin{aligned}
M_{b_{11}} &= m_1 + m_2 + m_3 \\
M_{b_{12}} &= m_2(-d_{1r} - d_{2f}) + m_3(-d_{1r} - l_2 - d_{3f}) \\
M_{b_{13}} &= -m_2 d_{2f} + m_3(-d_{3f} - l_2) \\
M_{b_{14}} &= -m_3 d_{3f} \\
M_{b_{21}} &= m_2(-d_{1r} - d_{2f}) + m_3(-d_{1r} - l_2 - d_{3f}) \\
M_{b_{22}} &= I_{z_1} + m_2(-d_{1r} - d_{2f})^2 + I_{z_2} + m_3(-d_{1r} - l_2 - d_{3f})^2 + I_{z_3} \\
M_{b_{23}} &= -m_2 d_{2f}(-d_{1r} - d_{2f}) + I_{z_2} + m_3(-d_{3f} - l_2)(-d_{1r} - l_2 - d_{3f}) + I_{z_3} \\
M_{b_{24}} &= -m_3 d_{3f}(-d_{1r} - l_2 - d_{3f}) + I_{z_3} \\
M_{b_{31}} &= -m_2 d_{2f} + m_3(-d_{3f} - l_2) \\
M_{b_{32}} &= -m_2 d_{2f}(-d_{1r} - d_{2f}) + I_{z_2} + m_3(-d_{3f} - l_2)(-d_{1r} - l_2 - d_{3f}) + I_{z_3} \\
M_{b_{33}} &= m_2 d_{2f}^2 + I_{z_2} + m_3(-d_{3f} - l_2)^2 + I_{z_3} \\
M_{b_{34}} &= -m_3 d_{3f}(-d_{3f} - l_2) + I_{z_3} \\
M_{b_{41}} &= -m_3 d_{3f} \\
M_{b_{42}} &= -m_3 d_{3f}(-d_{1r} - l_2 - d_{3f}) + I_{z_3} \\
M_{b_{43}} &= -m_3 d_{3f}(-d_{3f} - l_2) + I_{z_3} \\
M_{b_{44}} &= m_3 d_{3f}^2 + I_{z_3} \\
M_{b_{55}} &= M_{b_{66}} = 1 \\
M_{b_{15}} &= M_{b_{16}} = M_{b_{25}} = M_{b_{26}} = M_{b_{35}} = M_{b_{36}} = M_{b_{45}} = M_{b_{46}} = M_{b_{51}} = ... \\
M_{b_{52}} &= M_{b_{53}} = M_{b_{54}} = M_{b_{56}} = M_{b_{61}} = M_{b_{62}} = M_{b_{63}} = M_{b_{64}} = M_{b_{65}} = 0
\end{aligned}
$$

and,

$$
\begin{aligned}
A_{b_{11}} &= \frac{1}{p}(-C_{11} - C_{12} - C_{13} - d_{2r} - C_3) \\
A_{b_{12}} &= \frac{1}{p}(-C_{11} l_{11} + C_{12} * l_{12} + C_{13} l_{13} - d_{2r}(-d_{1r} - d_{2f} - l_{22}) ... \\
&- C_3(-d_{1r} - l_2 - d_{3f})) - p(m_1 + m_2 + m_3) \\
A_{b_{13}} &= \frac{1}{p}(-d_{2r}(-d_{2f} - l_{22}) - C_3(-d_{3f} - l_2 - l_{32})) \\
A_{b_{14}} &= \frac{1}{p}(-C_3(-d_{3f} - l_{32})) \\
A_{b_{15}} &= d_{2r} + C_3 \\
A_{b_{16}} &= C_3
\end{aligned}
$$

$$A_{b_{21}} = \frac{1}{p}(-C_{11}l_{11} + C_{12}l_{12} + C_{13}l_{13} - d_{2r}(-d_{1r} - d_{2f} - l_{22})...$$
$$- C_3(-d_{1r} - l_2 - d_{3f} - l_{32}))$$
$$A_{b_{22}} = \frac{1}{p}(-C_{11}l_{11}^2 - C_{12}l_{12}^2 - C_{13}l_{13}^2 - d_{2r}(-d_{1r} - d_{2f} - l_{22})^2...$$
$$- C_3(-d_{1r} - l_2 - d_{3f})(-d_{1r} - l_2 - d_{3f} - l_{32}))...$$
$$+ p(m_2d_{1r} + m_2d_{2f} + m_3d_{1r} + m_3l_2 + m_3d_{3f})$$
$$A_{b_{23}} = \frac{1}{p}(-d_{2r}(-d_{2f} - l_{22})(-d_{1r} - d_{2f} - l_{22})...$$
$$- C_3(-d_{3f} - l_2 - l_{32})(-d_{1r} - l_2 - d_{3f} - l_{32}))$$
$$A_{b_{24}} = \frac{1}{p}(-C_3(-d_{3f} - l_{32})(-d_{1r} - l_2 - d_{3f} - l_{32}))$$
$$A_{b_{25}} = d_{2r}(-d_{1r} - d_2f - l_{22}) + C_3(-d_{1r} - l_2 - d_{3f} - l_{32})$$
$$A_{b_{26}} = C_3(-d_{1r} - l_2 - d_{3f} - l_{32})$$
$$A_{b_{31}} = \frac{1}{p}(d_{2r}(d_{2f} + l_{22}) + C_3(d_{3f} + l_2 + l_{32}))$$
$$A_{b_{32}} = \frac{1}{p}(d_{2r}(-d_{1r} - d_{2f} - l_{22})(d_{2f} + l_{22})...$$
$$+ C_3(-d_{1r} - l_2 - d_{3f})(d_{3f} + l_2 + l_{32})) + p(m_2d_{2f} + m_3d_{3f} + m_3l_2)$$
$$A_{b_{33}} = \frac{1}{p}(d_{2r}(-d_{2f} - l_{22})(d_{2f} + l_{22}) + C_3(-d_{3f} - l_2 - l_{32})(d_{3f} + l_2 + l_{32}))$$
$$A_{b_{34}} = \frac{C_3}{p}(-d_{3f} - l_{32})(d_{3f} + l_2 + l_{32})$$
$$A_{b_{35}} = \frac{1}{p}(-d_{2r}(d_{2f} + l_{22}) - C_3(d_{3f} + l_2 + l_{32}))$$
$$A_{b_{36}} = \frac{1}{p}(-C_3(d_{3f} + l_2 + l_{32}))$$
$$A_{b_{41}} = \frac{C_3}{p}(d_{3f} + l_{32})$$
$$A_{b_{42}} = \frac{C_3}{p}(-d_{1r} - l_2 - d_{3f})(d_{3f} + l_{32}) + m_3d_{3f}p$$
$$A_{b_{43}} = \frac{C_3}{p}(-d_{3f} - l_2 - l_{32})(d_{3f} + l_{32})$$
$$A_{b_{44}} = \frac{C_3}{p}(-d_{3f} - l_{32})(d_{3f} + l_{32})$$
$$A_{b_{45}} = -C_3(d_{3f} + l_{32})$$
$$A_{b_{46}} = -C_3(d_{3f} + l_{32})$$

$A_{b_{53}} = A_{b_{64}} = 1$
$A_{b_{51}} = A_{b_{52}} = A_{b_{54}} = A_{b_{55}} = A_{b_{56}} = A_{b_{61}} = A_{b_{62}} = A_{b_{63}} = A_{b_{65}} = ...$
$A_{b_{66}} = 0$